TECHNOLOGICAL EDUCATIONAL INSTITUTE OF CRETE

BRANCH OF CHANIA

DEPARTMENT OF NATURAL RESOURCES AND ENVIROMENT

SECTION OF WATER RESOURCES AND GEOENVIROMENT

LABORATORY OF GEOPGYSICS AND SEISMOLOGY

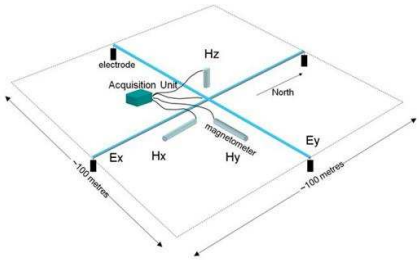

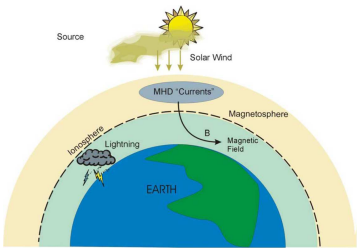

BACHELOR THESIS

Magnetotelluric monitoring: case studies of Agri valley (southern Italy) and Omalos (Western Crete, Greece)

by Aggeliki Karvouni

CHANIA 2013

ACKNOWLEDGEMENTS

I wish to thank Despina Kalisperi who was the first person to introduce me to Magnetotellurics, which was the subject of my thesis. Furthermore I would like to thank my supervisors Dr. Vincenzo Lapenna and Dr. Filippos Vallianatos who gave me the chance to transact my thesis in the Institute of Methodologies for Environmental Analysis of the National Research Council of Italy (I.M.A.A. C.N.R.) and finally I would like to thank most of all Gerardo Romano who was my advisor throughout the process of my thesis, providing me all the information and knowledge I needed to execute every stage of it!!!

ABSTRACT

This work concerns the implementation of Magnetotelluric Method one of the most consolidated Electromagnetic Methodologies of Geophysical prospection, based on the Earth's natural electromagnetic field, in the investigation and study of applying the Remote Reference Method.
In this thesis, it has been studied thoroughly the physical principles and the measurement techniques of magnetotelluric method and also the principles of operation and the different configuration modes of the advanced magnetotelluric measurement system MT24/LF of EMI along with its electric and magnetic sensors. The MT measurements have been conducted at two permanent MT-stations in Omalos, Crete, Greece owned by the Laboratory of Geophysics and Seismology at the Department of Natural Resources & Environment of Technological Educational Institute of Crete and in Agri Valley, Bascilicata, Italy installed by the Institute of Methodologies for Environmental Analysis of the National Research Council of Italy (I.M.A.A. C.N.R.). The MT measurements were analyzed and processed with the Egbert's robust program, resulting to the construction of the apparent resistivity and phase curves versus frequency using Matlab.

ΠΕΡΙΛΗΨΗ

Η πτυχιακή εργασία αφορά στην εφαρμογή της Μαγνητοτελλουρικής Μεθόδου, μία από τις πιο εδραιωμένες Ηλεκτρομαγνητικές Μεθοδολογίες Γεωφυσικής διασκόπησης με αξιοποίηση του φυσικού ηλεκτρομαγνητικού πεδίου της Γής στη διερεύνηση και μελέτη εφαρμώζοντας Remote Reference Method. Στην πτυχιακή αυτή, μελετήθηκαν διεξοδικά οι φυσικές αρχές και οι τεχνικές μετρήσεων της μαγνητοτελλουρικής μεθόδου καθώς και η αρχή λειτουργίας και οι τρόποι διαμόρφωσης του προηγμένου μαγνητοτελλουρικού συστήματος μέτρησης MT24/LF του οίκου EMI μετά των αισθητήρων ηλεκτρικού και μαγνητικού πεδίου που το συνιστούν. Οι MT μετρήσεις πραγματοποιήθηκαν σε δύο μόνιμους Μαγνητοτελλουρικούς σταθμούς στον Ομαλό, Κρήτη, Ελλάδα που ανήκει στο Εργαστήριο Γεωφυσικής και Σεισμολογίας του παραρτήματος Φυσικών Πόρων και Περιβάλλοντος του ΤΕΙ Κρήτης και Agri Valley, Βασιλικάτα, Ιταλία εγκατεστημένο απο το Ινστιτούτο Μεθοδολογιών για την Περιβαλλοντική Ανάλυση του Εθνικού Συμβουλίου Ερευνών της Ιταλίας. Τα μαγνητοτελλουρικά δεδομένα έτυχαν ανάλυσης και επεξεργασίας μέσω του προγράμματος του Egbert όπου και προέκυψαν οι καμπύλες φαινόμενης αντίστασης και φάσης συναρτήσει της συχνότητας, χρησιμοποιώντας το Matlab.

Contents

INTRODUCTION

Electrical conductivity is one of the most widely varying physical properties of Earth. While the seismic velocity and density of rocks that comprise Earth's crust typically vary at most by about one order of magnitude and more typically by a factor of 2, the electrical conductivity (and its reciprocal resistivity) typically varies by many orders of magnitude. The large contrasts that result make electrical conductivity an attractive tool for geophysicists interested in exploring the structure and physical state of Earth's interior. The electrical conductivity of any rock depends on the its composition, temperature, porosity, permeability and pore fluid content, and so knowledge of the electrical conductivity distribution of subsurface structures can provide information on a wide range of other physical and geological properties.

Temperature, pressure, physical and chemical state, porosity and permeability, as well as the frequency at which measurements are made can all play a crucial role in determining the electrical resistivity exhibited by rocks and minerals. Conduction (the transmission of electrical currents by free charge carriers) occurs in rocks and minerals via three principal electrical charge propagation mechanisms: electronic, semi-conduction and electrolytic. Electronic conduction occurs in metallic ore minerals (e.g. magnetite, hematite) which contain free electrons that can transport charge. Electronic conduction is most significant in the Earth's core. The conductivity of the amorphous graphite that occurs in the Earth's crust is lower than the conductivity of metallic ores, but higher than the conductivity of natural semi-conductors or electrolytes. Semi-conduction occurs in poor conductors containing few free charge carriers. Semi-conduction is expected to dominate in mantle minerals such as olivine. Electrolytic conduction occurs in a solution containing free ions, such as saline water which is an electrolyte of particular relevance to crustal EM studies, furthermore as electrolyte can act as partial melt generated by enhanced temperatures, adiabatic decompression or asthenosperic upwelling in active tectonic regions.

One well established technique for imaging electrical conductivity structure is the magnetotelluric (MT) method. This technique utilizes the natural time variations of Earth's magnetic field in the period range of about 0.001 to 100,000 s as a source of excitation energy. The time variations of the magnetic field induce a corresponding electric field within Earth that is proportional to the conductivity structure. The physics of the method involves the diffusion

equation and so the resolution is less than for methods based on the wave equation (seismology, ground penetrating radar), however, the wide period range that can be utilized makes the method sensitive to structures at crustal depths of a few meters to mantle depths of 100's of kilometres. The development of the magnetotelluric (MT) method has taken considerable leaps in the 50 years since it was first proposed [Tikhonov, 1950; Cagniard, 1953]. Advancements in instrumentation, data processing and modelling have resulted in many significant land based problems being solved using the magnetotelluric method.

The magneto-telluric method, which is the subject of this paper, answers the ever increasing need for quantitative results. Actually, it is not a strictly electrical method, but rather a combination of telluric and magnetic methods, a combination from which the name of the technique has been derived. Essentially, the magneto-telluric method involves the comparison, preferably at one and the same place, of the horizontal components of the magnetic and electric fields associated with the flow of telluric currents. The method offers all the advantages of the telluric method and even improves on it with respect to flexibility, speed, and economy. In addition, it offers the inestimable benefit of making possible, in most cases where the bedding is horizontal, a truly quantitative interpretation.

In recent years, the MT method proved to be effective in a broad range of applications regarding the Earth's interior studies like crustal studies or faults imaging. A quite recent application of the method concerns the continuous monitoring of seismic active areas to detecting anomalous temporal patterns of the MT transfer function connected to the seismic activity.

The effectiveness of this last application of the MT method is still under investigation and it is part or the main topic of some international project (i.e. IPOC - Integrated Plate boundary Observatory Chile; MT-GEAR - MagnetoTellurics in studying Geodynamics of the Hellenic Arc; Agri Valley (Italy) MT monitoring) and crucial point is the capability to obtain unbiased and stable MT estimates. The continuous growing of the antropization level of the lands, and hence of the cultural electromagnetic noise, makes this task particularly hard and force the scientists to find and experiment always new data analysis techniques. The presence of the cultural related dynamics affecting the MT monitoring can easily lead, in fact, to a false interpretation of magnetotelluric data and to the impossibility of detecting the presence of resistivity variations within the subsoil.

Among all the MT noise reduction techniques, the Remote Reference method (RR) is well known as one of the most effective. It allows a minimization of the effects of coherent noise (ie. DC train noise) on the MT estimates by means of acquiring simultaneous EM fields in the “local site” (the one that has to be investigated) and the “remote site” (usually considered as quiet site) with a spacing between the two sites of a few hundreds of kilometers.

In this thesis, it will be explored the possibility of applying the Remote Reference method and along with its advantage between two monitored sites: Omalos, Crete, Greece and Agri Valley, Basilicata, Italy. The novelty of this topic will be represented by the distance between the local and the remote station (~ 1000 km), an order of magnitude greater than in the usual application of the RR techniques.

The structure of the thesis will be:

- Chapter I: The geological outline of the areas of interest.
- Chapter II: A description of the MT method (applications, sources, fundamental equations, transfer function, dimensionality models).
- Chapter III: A description of the MT instruments used for data recording.
- Chapter IV: Analysis performed on the data
- Chapter V: An explanation of the results that obtained during the processing in Chapter IV.

CHAPTER I: GEOLOGICAL SETTING OF THE STUDY AREA

Investigated area

In this thesis it will be analyzed MT data collected in two different areas: Agri valley (Basilicata, Italy) and Omalos region (Crete, Greece).

Since 2003, a MT monitoring network has been installed by the Institute of Methodologies for Environmental Analysis of the National Research Council of Italy (I.M.A.A. C.N.R.) in the Agri Valley (Balasco et al., 2008). The site has been chosen due to the presence of: i) a coherent fault system N120 trending left-lateral strike-slip fault which can be related to some of the most destructive seismic events occurred in the southern Italy (i.e. the Earthquake occurred on December 1857 (I=XI MCS) (Mallet, 1862), ii) the presence of great hydraulic engineering structures (Pertusillo and Marsico Nuovo Dams) and iii) for the intense exploration of oil and natural gas, operated since the 1980s. Among all the MT stations of the network, Tramutola station plays a key role. It is placed in southeastern flank of the Valley and is the only one in the MT network which, at present time, can be considered permanent.

TEI of Crete and more specifically the Laboratory of Geophysics and Seismology has selected the plateau of Omalos as one of the best location for the placement of the permanent MT station, far away from human activity, current sources, pipelines or metallic fences which can create problems for the measurements.

1.1GEOLGICAL OUTLINE OF OMALOS.CRETE, GREECE

Fig.1.1: Panoramic picture of Omalos plateau

Lefka Ori (The White Mountains) is a mountain range located in Western Crete in the Chania prefecture. The island of Crete is located north of the Hellenic trench and is the largest of the Greek islands and the fifth-largest island in the Mediterranean Sea.

The geological framework consists largely of nappes of contrasting lithologies and metamorphism that were stacked southwards during an Oligocene to early Miocene N-S compression (Pomoni F. and Karakitsos V., 2002) The White Mountains is the largest mountain range of Crete and is formed in total from marble, limestone and dolomite - rocks whose main component is calcium carbonate. In total, they were formed million years ago, in the sea from the dissolved calcium carbonate which was swept away from the earth's rocks by rainfall.

Geology of Omalos

In total, the core of the mountain range is comprised primarily of two main groups of rocks: Plattenkalk limestone and Tripali (Vafidis A. et al,. 2004) The most important and the one that occupies the largest volume, is Plattenkalk limestone. These are the rocks that form the ridge

(backbone) on which all the other groups of rocks are found, and in addition, they are the deepest rocks that are known in Crete, since we do not know what lays underneath them.

Apart from the Plattenkalk limestone rocks, there are some other groups of rocks in the White Mountains. These are the recrystallized limestone of Tripali, the shale, mainly, rocks of the Phyllite-Quartzite group, and the Tripoli limestone (Fasoulas Dr. G. 2004). The Tripali rocks appear only in western Crete and are the distinctive white limestone of the peaks of the White Mountains that cover the Plattenkalk limestone, or the brecciated limestone with the cavities encountered from the village of Lakkoi until Omalos, or at Mount Tripali, on the east of the mountain range (Hamdan et al, 2012) Their age is between 200 and 140 million years. The rest of the rocks, also cover the Plattenkalk limestone, but are rarest, found mainly on the east and west margins of the mountain range. The "White Mountains" have got their name from the perpetual white or off white color of their peaks as the off white of limestone during the summer and fall interchanges with the snow that covers the peaks until late in spring.

Omalos Plateau (Fig. 1.1) is in the centre of the Cretan mountains named Lefka Ori and is located 38km south of Chania at an altitude ranging from 1,040 to 1,250 meters, surrounded by the high peaks of the White Mountains. In the winter, the plateau it is frequently covered by snow.

The Omalos plateau is located on the fault separating the Trypali nappe from the underlying limestones. The area consists of three geological units (Fig. 1.2) (Lydakis et al. 2005)

i. Neocene and Quaternary formations
ii. Trypali unit (Regarding to the transition from the underlying metamorphic carbonaceous formations to Trypali Unit and the metaclastic formations of Phyllite/Quartzite Series, Creutzburg and Seidel (1975) came up with a surprising conclusion. Although in several positions they notice that Trypali Unit seems to pass gradually to Phyllite/Quartzite Series, they describe Trypali Unit as a separate structural unit of the External Hellenides)
iii. Plattenkalk group.

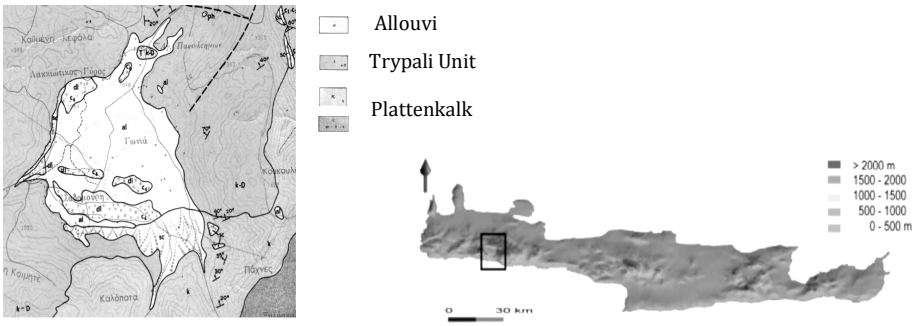

Figure 1.2: Location of the Omalos polje-plateau and geological outline of the area. (Geological map after Tataris and Christodoulou 1969)

The plateau consists mainly of marl and conglomerates which lie on the Trypali limestones. The rock formations around the Omalos plateau are mainly part of the Trypali unit and less of the Plattenkalk group (Manutsoglu Spyridonos, Soujon, Jacobshagen, 2001). The Plattenkalk Group represents the lowermost known tectonic unit beneath the nappe pile of Crete and their formation has been involved in the tectonometamorphic process during the Oligocene-Miocene.

1.2 GEOLGICAL OUTLINE OF AGRI VALLEY, ITALY

Fig. 1.3: Panoramic picture of Agri Valley.

The Apennines are a mountain range consisting of parallel smaller chains extending c. 1,200 km along the length of peninsular Italy. The Southern Apennines fold-and-thrust belt accreted from Miocene to Early Pleistocene in the westward directed subduction of the Adriatic-Ionian lithosphere slab [Malinverno and Ryan, 1986; Patacca et al., 1990]. Since Middle Pleistocene (500–700 ka) [Hippolyte et al., 1994], NE-SW extension together with regional uplift has affected the axial sector of the Apennines, leading to the opening of intermontane basins along NW-striking high-angle normal and oblique faults [Cinque et al., 1993; Hippolyte et al., 1994]. However, disruption of pre-Quaternary constructional structures is limited since they still shape the mountain landscape. Seismicity and all stress indicators indicate that the extensional stress regime is on-going [Pondrelli et al., 2006; Montone et al., 2004]. The development of the Southern Apennines accretionary prism occurred through the off-scraping and incorporation at the subduction zone of the Meso-Cenozoic passive margin sedimentary covers, which overlay the subducted Apulo-Adriatic crystalline basement, and the associated foredeep deposits. Beneath the mountain chain the Apulian platform shallow water carbonates are deformed to shape a buried antiformal stack (Fig. 1.4)

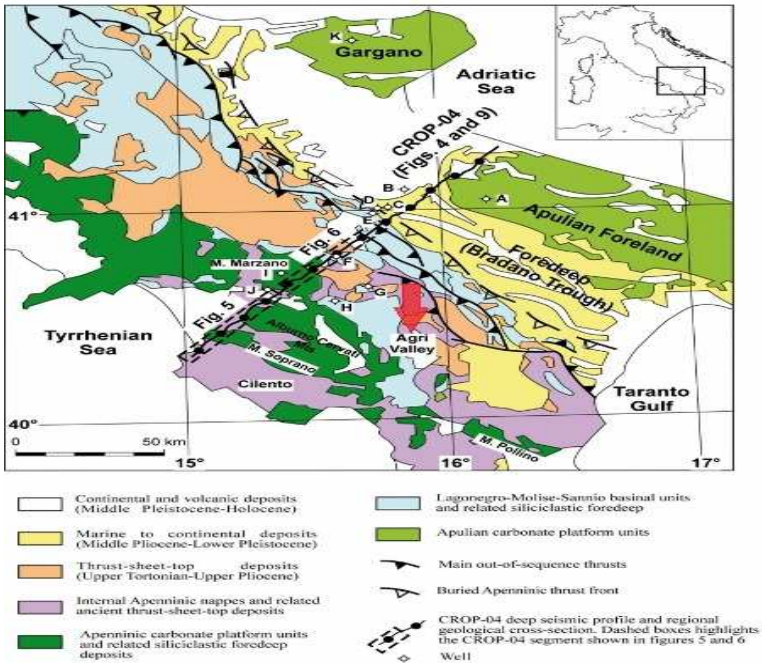

Figure 1.4: Simplified geological map of the Southern Apennines (modified after Patacca *et al.*, 1992 and Patacca and Scandone 2007). The location of the geological cross section and segments of the CROP-04 profile shown in this paper are highlighted. Letters identify relevant wells (A, Puglia 1; B, Gaudiano 1; C, Bellaveduta 1; D, Lavello 5; E, Lavello 1; F, S. Fele 1;G, M. Foi 1; H, Vallauria 1; I, S. Gregorio Magno 1; J, Contursi 1; K, Gargano 1), (Beltrando M., et al 2010)

Geology of Agri Valley

The Val d'Agri region hosts one of the largest intermontane basins of the Apennines (Fig. 1.3). Agri Valley is a NW-SE intermountain basin formed during Quaternary age surrounded by mountains, bounded by border faults of Apennine flow, filled up by rubble-alluvial materials. (Improta L. et al 2010) The valley is hemmed by mountains made up of geological formations of limestone nature belonging to Carbonate Platform Units overlapping Basin Units of Lagonegro, made up of limestone-silicon-marly formations, and by terrigenous formations of sandy-conglomerate and silicon-marly nature that testify the dismantling of Apennines range and the deposition of sediments in foredeep coming from the unborn peninsular arch. The prequaternary bedrock is composed by Mesozoic-Cenozoic shallow-water and slope carbonates, mainly outcropping along the west site of the basin, while toward east and south-east, the bedrock is

formed by Tertiary silico-clastic sediments (Priore A., Geology and geomorphology of Upper Agri Valley. Available on: http://www.grumentum.net/en/geologia-e-geomorfologia-dellalta-val-dagri) The intermountain basin of the Agri Valley represents one of the higher seismic and environmental hazard areas of the Southern Apennines. in historic and recent years this area has been hit by many seismic events, sometimes destructive, like that which occurred on December 1857(I=XI MCS) (Mallet, 1862). This area is affected by a coherent fault system N120 trending left-lateral strike-slip fault. The seismicity of the valley is basically attributable to active faults in the area. The seismogenetic faults, structures of weakness in the earth's crust, often create dangerous situations causing earthquakes of different magnitude. The Agri Valley is, as already mentioned above, a tectonic depression bounded by faults with Apennines direction and other faults that interrupt the previous ones with anti-Apennines direction. The evidences of these structures can be followed on the edges of the valley in a fairly marked way, especially considering the change of slope between the mountainsides and the valley bottom. In Fig. 2.5, a structural map of the Agri Valley is showed with the location of all the MT stations composing the monitoring network. (Giano S. I. et, al. 2000)

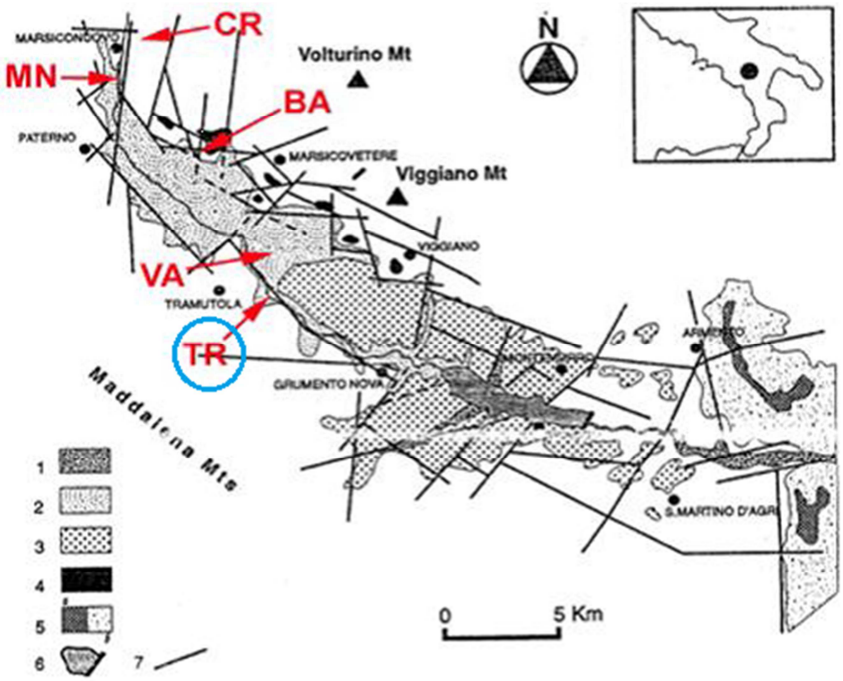

Fig. 1.5: structural map of the Agri Valley; red arrows indicate the position of the MT stations: CR (Campo Reale site), MN (Marsico Nuovo site), BA (Barricelle site), VA (Villa d'Agri site) and TR (Tramutola site).

CHAPTER II: THE MAGNETOTELLURIC METHOD

Magnetotellurics (MT) is a passive exploration technique that utilizes a broad spectrum of naturally occurring geomagnetic variations as a power source for electromagnetic induction in the Earth and was introduced by the French geophysicist Louis Cagniard and Russian geophysicist Andrey Nikolayevich Tikhonov in the early 1950s. It allows imaging the distribution of the electrical resistivity properties into the subsoil based on the propagation of electromagnetic (EM) waves into the ground, the MT investigation depth (from 300m below ground down to 10,000m or deeper) is strictly connected to the ability of EM waves to penetrate into the Earth. A raw estimate of this feature can be obtained by considering the so called "electromagnetic skin depth relation" that describes the exponential decay of electromagnetic fields as they diffuse into a medium is: (Bahr K. and Simpson F. 2005)

$$\delta\,(T) = (T/\pi\mu\bar{\sigma})^{1/2} \qquad (2.1)$$

where δ (T) is the electromagnetic skin depth in meters at a given period T, $\bar{\sigma}$ is the average conductivity of the medium penetrated and μ is magnetic permeability. In MT studies the electromagnetic skin depth is generally equated with the penetration depth of electromagnetic fields into the Earth. Studying the Earth we can see that μ is usually assigned to the free-space value ($\mu_{0=}4\pi \times 10^{-7} Hm^{-1}$), so equation (2.1) can be approximated as:

$$\delta\,(T) \approx 500\sqrt{T\rho_{\alpha}} \qquad (2.2)$$

where ρ is the apparent resistivity or the average resistivity of an equivalent uniform half-space. Using the equations (2.1) and (2.2) we presume that for a given sounding period, the depth which can be achieved by passive EM sounding is dictated by the average conductivity of the overlying sample of Earth that is penetrated. With advances in instrumentation, processing and modelling, MT has become one of the most important tools in deep Earth research.

2.1 MT APPLICATIONS

The magnetotelluric method, since its inception during 50's, had a phenomenal growth, both in development of the methodology and also the capability of the method for solving different geological problems. After the first papers on MT theory, it took about 20 years before MT was brought into practice. Since then, MT has developed fast in all fields (e.g., theory, field instrumentation and interpretation

Philosophy) and the scientific and industrial interest grew rapidly. Within only a few decades, interpretation philosophies, processing tools, modelling and inversion codes evolved from a one-dimensional (1D) Earth to a three-dimensional (3D) understanding, although the latter is still in its infancy regarding modelling and inversion. Today MT is used for scientific purposes as well as for industrial exploration. Industry seems to have recognized the advantages of MT, which is useful in areas where seismics cannot be practically or economically applied or where the target is characterized by an electrical properties contrast, rather than a change in seismic velocity or a density contrast. The environmental impact of MT is negligible and the costs are relative low when using the method for exploration.

Due to the huge frequency range from 10^{-5}- 10^{4} Hz and therefore depths of penetration from 10 m to up to 200 km, MT can be used for a large number of applications, such as:

1. Deep crustal and mantle studies: The aim of crustal and mantle studies is usually to understand the structure and tectonic history of a certain region on a large scale. Therefore these kinds of studies are mostly conducted by academic institutions although the results can also help the mining industry to understand fundamental properties of that region.
2. Geothermal studies: Geothermal studies are of interest to both academia and industry. Examining the structure of geothermal areas helps to understand basic properties of these systems and the connection to large scale tectonic processes, but also allows energy companies to identify interesting regions for geothermal power generation (Harinarayana T., 2008)
3. Environmental studies: Usually shallow borehole measurements are used to investigate the extent and to monitor changes within waste sites. This technique, however, is relatively expensive.

4. Oil and mineral exploration: MT methods are important cheap supplementary methods to seismic surveys for petroleum exploration. Petroleum and natural gas are often trapped in pockets between rock and salt that were formed by the upward movement of salt towards the surface, penetrating and bending the existing rock. Due to this fact, mapping the top and bottom of salt structures is important to identify the location of reservoirs.

These examples of MT applications also show that most analyses of MT data are still performed with 2D inversion schemes and only rarely 3D tools are utilized. This is due to limited computer power, limited availability of 3D inversion codes and generally lower requirements in terms of number of stations for 2D surveys. With current computer power and a greater variety of 3D inversion codes available it is starting to become mostly a matter of experimental design and costs whether 3D methods can be used or not.

2.2 THE MAGNETOTELLURIC SOURCES

Naturally occurring geomagnetic variations, source of the MT method, range between periods of 10^{-3} s and 10^{5} s and are generated by two different sources, which strongly differ in amplitude and in their time-dependent behavior: the thunderstorm activity (for period shorter than 1 s) and by the interaction of the solar wind with the Earth magnetosphere (Bahr and Simpson, 2005)

The electromagnetic waves emitted by individual lightning strokes get partially trapped in the waveguide, (the signals traveling within the waveguide are also known as spherics) formed between the conductive ionosphere, the part of the atmosphere with the largest concentration of ions extending from 100 to 250 km above the Earth's surface, and the Earth. These waves can travel long distances and the lightning somewhere in the world is enough to provide a continuous source at any location of the Earth's surface. The measured field at the surface of the Earth is a superposition of waves generated from individual lightnings and the exact characteristics of the electromagnetic fields depends on the size, shape and the nature of the boundaries of the waveguide. As long as the measurements are far away from the individual thunderstorms this superposition can be considered as a plane wave.

From 1 s to 10^{5} s, the geomagnetic fluctuations are linked to the interactions between solar wind and the Earth's magnetosphere (magnetopause) and ionosphere (Fig. 2.1). Solar wind is a continuous stream of plasma, carrying a weak magnetic field. Constant pressure of the solar wind onto the magnetosphere causes compressions on the sun-directed side and a tail on the night-side. Due to changes in density, velocity and strength of the solar wind, the Earth's magnetosphere is subject to varying distortions and changes in the magnetic field. On the day side of the Earth, soft x-rays and ultraviolet light cause ionization of air molecules in the ionosphere at altitudes of 80-120 km. Solar heat induces thermal convection of the ionized air molecules and thus establishes large-scale electric currents acting as magnetic fields sources.

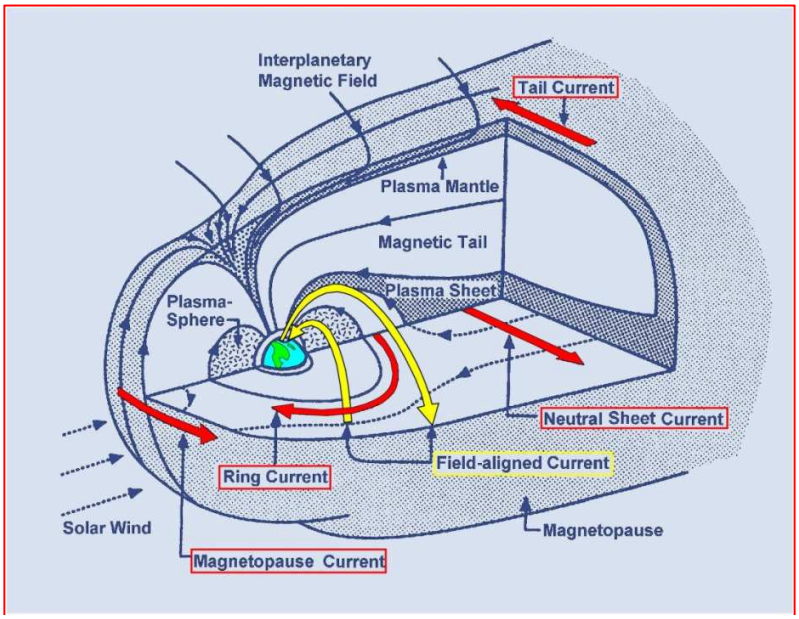

Figure 2.1.: A sketch of the magnetosphere (modified from Kivelson and Russel (1995)

The combined effects of the two above mentioned phenomena create a quite uniform plane waves (see appendix A) source in the period range [10^5 s, 10^5 s] for the final MT spectrum which is shown in Figure 2.2

The overlapping of the two mechanisms responsible for the generation of the MT source is not complete; around 1 s, in the limit between thunderstorm activity and solar wind-magnetosphere interaction, a so-called “dead-band”-characterized by low amplitude MT signals can be observed. MT measurements in this frequency range usually suffer from poor data quality.

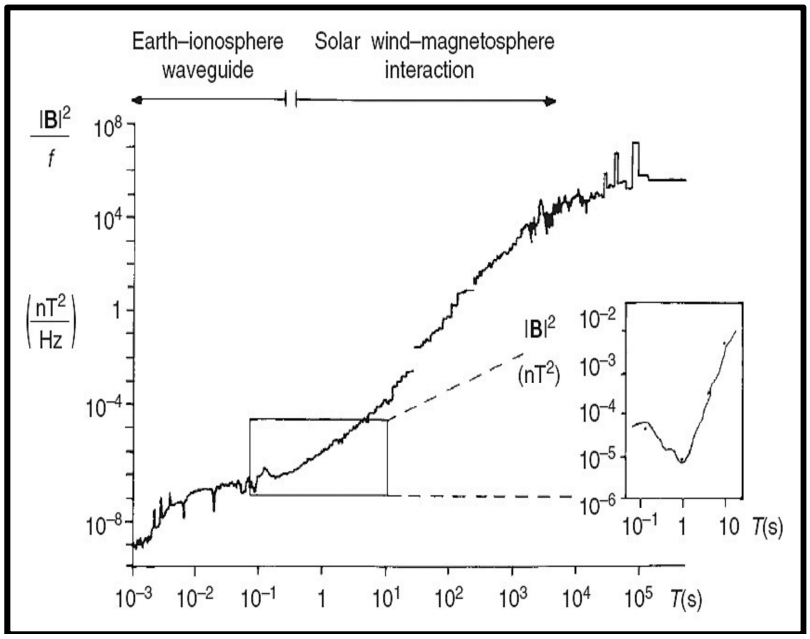

Figure 2.2.: Power spectrum of natural magnetic variations. The inset shows the minimum of the power spectrum in the dead-band (modified from Simpson and Bahr, 2005).

2.3 THE FUNDAMENTAL EQUATIONS OF THE MT METHOD

To derive the equations useful to describe the electromagnetic wave propagation in a medium is to start by Maxwell's equations that describe the behavior of both the electrical and magnetic fields and their interaction.

Therefore, at any frequency, the physical principles of the MT method are based on these four equations: (Arnason K. 2007)

$$\vec{\nabla} \cdot \vec{D} = \rho \qquad \text{Gauss's Law (2.3)}$$

$$\vec{\nabla} \cdot \vec{B} = 0 \qquad \text{Gauss's Law for magnetism (2.4)}$$

$$\vec{\nabla} \times \vec{E} = -\frac{\partial \vec{B}}{\partial t} \qquad \text{Faraday's Law (2.5)}$$

$$\vec{\nabla} \times \vec{H} = \vec{J} + \frac{\partial \vec{D}}{\partial t} \qquad \text{(Ampere-Maxwell Law) (2.6)}$$

where $\vec{E}$ (V/m) and $\vec{H}$ (A/m) are the electric and magnet fields, $\vec{B}$ (T) is the magnet induction, $\vec{D}$ (C/m^2) is the electric displacement and ρ(C/m^3) is the electric charge density owing to free charges. $\vec{J}$ (J=σE) and $\partial\vec{D}/\partial t$ (A/m^2) are the current density and displacement current respectively, σ(S/m) is the electrical conductivity and also $\rho = 1/\sigma$ (Ωm), ε (F/m) is the dielectric permittivity and μ (H/m) is the magnetic permeability.

They are Gauss's law (Fig. 2.3) for the magnetic field (the magnetic field is source free, there are no free magnetic charges, i. e., magnetic monopoles do not exist [divB=0]) and Gauss's law for the electric field (the electric field or the electric displacement is a field with the charge density as its source [divD=q]), Faraday's law (any time variation of the magnetic field causes an electric vortex field) and Ampère's law(The magnetic field depends on the electrical current density of free charges and the time variation of the electric displacement.

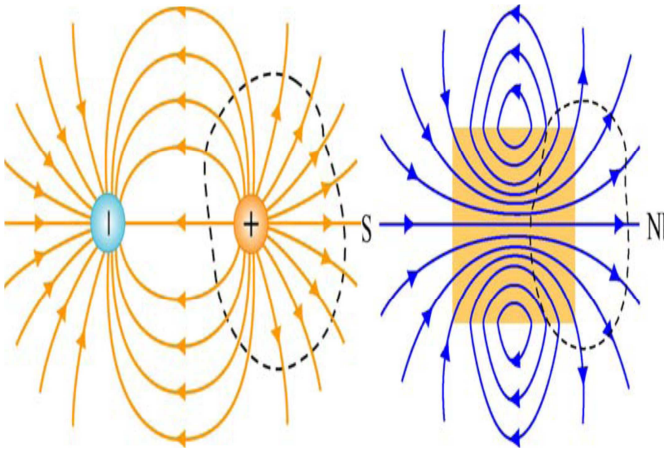

Figure 2.3.: Gauss's law for (a) electrostatics, and (b) magnetism

The vectorial magnitudes in Maxwell's equations can be related through their constitutive relationship:

(2.7)

(2.8)

(2.9)

Where σ(S/m) is the electrical conductivity, ε (F/m) is the dielectric permittivity and μ (H/m) is the magnetic permeability (2008, Basics of the Magnetotelluric Method, Gh. 1-3. Available on: http://digital.library.adelaide.edu.au/dspace/bitstream/2440/48492/6/02chapters1-3.pdf) The first constitutive equation is the Ohm's Law which relates the electric current density j to the electric field E by taking the material's property the conductivity σ into account.

The second constitutive equation, relates the electric field E to the electrical displacement D. Where ε is the electrical permittivity, which is given by the electrical permittivity of a vacuum = 8.854 As/Vm and the unitless, relative electrical permittivity which is specific to the material:

= ·

The relative electrical permittivity varies from = 1 for a vacuum to = 80.36 for water (at 20°C (Telford et al., 1990)).

The third constitutive equation describes the relation between the magnetic induction B, the magnetic intensity H and the magnetic permeability μ. The permeability μ is the degree of magnetization of a material that responds linearly to an applied magnetic field. If the medium is isotropic, permeability is a scalar, whereas for an anisotropic linear medium it becomes a second rank tensor. Magnetic permeability μ is a combination of the permeability of a vacuum μ_0 = $4\pi\times 10^{-7}$ Vs/Am and the unitless relative permeabilityμ_r, which is specific to the material:

$$\mu = \mu_r \cdot \mu_0$$

For most Earth materials, permeability is very close to the free-space (vacuum) value, except for those rocks containing a large quantity of iron.

For MT studies, variation in μ, of rocks are negligible compared with variations in bulk rock conductivities and free-space values can be assumed. Kao and Orr (1982) showed that the common assumption of μ = μ_0 can cause misleading interpretation of MT data if a layer of highly magnetized minerals is present. They demonstrated that a magnetized layer could be misinterpreted as an unmagnetized layer, which is (μr-times) more resistive and (μr-times) thicker than the magnetized one. This becomes a problem particularly when a local area hosting a mineral deposit, that has permeability many times higher than the free-space value μ_0, is studied using high frequencies.

In isotropic and homogeneous medium, Equations 1.8-9 allow us to rewrite eq.2-5,68 as follow: (σ: specific resistance [Sm-1]):

$$\vec{\nabla} \times \vec{E} = -\mu \frac{\partial H}{\partial t} \quad (2.10)$$

and

$$\vec{\nabla} \times \vec{H} = \sigma \vec{E} + \varepsilon \frac{\partial \vec{E}}{\partial t} \quad (2.11)$$

Taking the curl of eq. 2.10, and 2.11, using eq. 2.3, 4 and remembering that in a conductive medium there cannot be charge accumulation, it is possible to obtain the following two formulas:

$$\Rightarrow \quad \vec{\nabla} \times \left(\vec{\nabla} \times \vec{E}\right) = \vec{\nabla} \times \left(-\mu \frac{\partial H}{\partial t}\right)$$

$$\Rightarrow \vec{\nabla} \times \left(\vec{\nabla} \times \vec{H}\right) = \vec{\nabla} \times (\sigma \vec{E} + \varepsilon \frac{\partial \vec{E}}{\partial t})$$

After solving the above equation we conclude:

$$\nabla^2 \vec{H} = \sigma\mu \frac{\partial \vec{H}}{\partial t} + \varepsilon\mu \frac{\partial^2 H}{\partial t^2} \text{ (2.12)}$$

and

$$\nabla^2 \vec{E} = \sigma\mu \frac{\partial \vec{E}}{\partial t} + \varepsilon\mu \frac{\partial^2 E}{\partial t^2} \text{ (2.13)}$$

which are the wave equations in a conductive medium. In the left part of eqs. 2.12, 13 the two terms are linked to the conduction currents and to the displacement currents.

MT measurements rely on a source of energy diffusing through the Earth and which is exponentially dissipated. MT measurements yield to volume sounding because electromagnetic fields propagate diffusively. Therefore we can consider $\vec{E}$ and $\vec{H}$ as waves.

$$\vec{E}(\vec{r}, t) = E(\omega) e^{i\vec{k}\vec{r} + i\omega t} \qquad (2.14)$$

$$\vec{H}(\vec{r}, t) = E(\omega) e^{i\vec{k}\vec{r} + i\omega t} \qquad (2.15)$$

where k is the wavenumber, ω is the angular frequency (ω=2πf and f is the frequency f=1/T, (T=period)).

Replacing eq. 2.14 in eq. 2.13, it is possible to obtain:

$$\nabla^2 \vec{E} = \mu\sigma \frac{\partial}{\partial t}\left(E(\omega) e^{i\vec{k}\vec{r} + i\omega t}\right) + \mu\varepsilon \frac{\partial^2}{\partial t}\left(E(\omega) e^{i\vec{k}\vec{r} + i\omega t}\right) \qquad (2.16)$$

By taking each part of the left side separately, we have that:

$$\frac{\partial}{\partial t}\left(E(\omega) e^{i\vec{k}\vec{r} + i\omega t}\right) \Rightarrow \frac{\partial}{\partial t}\left(E(\omega) e^{i\vec{k}\vec{r}} \cdot e^{i\omega t}\right)$$

$$\Rightarrow E(\omega) e^{i\vec{k}\vec{r}} \cdot \frac{\partial e^{i\omega t}}{\partial t} \Rightarrow E(\omega) e^{i\vec{k}\vec{r}} \cdot (e^{i\omega t} \cdot i\omega) = i\omega E(\vec{r}, t)$$

$$\frac{\partial^2\left(E(\omega)e^{i\vec{k}\vec{r}+i\omega t}\right)}{\partial t^2}=\frac{\partial}{\partial t}\left(\frac{\partial\left(E(\omega)e^{i\vec{k}\vec{r}+i\omega t}\right)}{\partial t}\right)$$

$$=\frac{\partial}{\partial t}\left(i\omega\cdot\left(E(\omega)e^{i\vec{k}\vec{r}+i\omega t}\right)\right)$$

$$=\iota^2\omega^2\,E(\vec{r},t)$$

Except that:

$$i^2=-1$$

$$\Rightarrow\ -\omega^2E(\vec{r},t)$$

Ultimately solving Equation (2.16), we conclude that:

$$\nabla^2\vec{E}=i\omega\mu\sigma\vec{E}-\mu\varepsilon\omega^2\vec{E} \qquad (2.17)$$

and similarly for eq. 2.12:

$$\nabla^2\vec{H}=i\omega\mu\sigma\vec{H}-\mu\varepsilon\omega^2\vec{H} \qquad (2.18)$$

Depending on the medium a wave can travel, we can distinguish two cases:

1. For waves travelling in the vacuum or in a perfect isolator:

$\sigma\rightarrow 0$, so we have:

$$\nabla^2\vec{E}=-\mu\varepsilon\omega^2\vec{E} \qquad (2.19)$$

$$\nabla^2\vec{H}=-\mu\varepsilon\omega^2\vec{H}$$

2. For waves travelling in the Earth: (Hensir G.P., Arnason K. 2009)

$\sigma\approx 1-10^4$ S/m

$\omega=2\pi/T$ with $T\approx 10^{-4}-10^4$ seconds

we have $i\omega\mu\sigma \gg \mu\varepsilon\omega^2$, so we arrive in the Equations that apply in the MT method, which are:

(2.20)

Solution of Maxwell's equation in a particular case: Homogeneous half-space

The solution of eq. 217 and 2.18 can be easily derived in some simple cases; let us consider, for example, a polarized electromagnetic wave which propagates along z direction (where, z is the vertical direction, positive toward the center of the earth, fig (2.4).

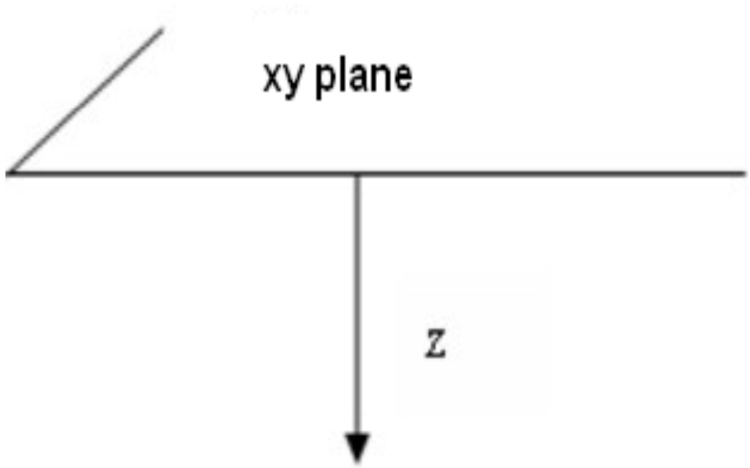

Figure 2.4.: A polarized electromagnetic wave which propagates along z direction.

Without losing of generality, we can consider a magnetic field directed along the *y* direction

. Equation 1.15 become, taking z as the direction of the propagation, as:

(2.21)

After some simple calculus, it is possible to obtain from the eq. 2.20:

(2.22)

It can be seen that the general solution of the above equation can be written as:

$$H_y(z,t) = H_0 e^{(i\omega t \pm (1+i)\alpha z)} \quad (2.23)$$

where, $\alpha = \left(\frac{\omega\mu\sigma}{2}\right)^{\frac{1}{2}}$

For $z \to \infty$, H_y has to remain finite, we must discard the positive solution obtaining:

$$H_y(z,t) = H_0 e^{(i\omega t - (1+i)\alpha z)}$$
$$\Rightarrow H_0 e^{-\alpha z} \cdot e^{i(\omega t - \alpha z)}$$
$$\Rightarrow H_0 e^{-\alpha z} \cdot \left(cos(\omega t - \alpha z) + i\, tan(\omega t - \alpha z)\right)$$

And, considering only the real part:

$$\Rightarrow H_y(z,t) = H_0 e^{(-\alpha z)} \cdot cos(\omega t - \alpha z) \quad (2.24)$$

A similar result can be obtained for the electric field $\vec{E} = (E_x, 0, 0)$.

The factor $e^{-\alpha z}$ represents the exponential decay of the wave amplitude as function of the depth z. The depth δ, for which the wave amplitude shades by a factor e^{-1}, is called "skin depth" and it is given by the following formula (Vozoff, 1991):

$$\delta[km] \approx 0{,}5\sqrt{\rho[\Omega m]\, T[s]}$$

δ gives indication of the reached investigation and is the equation that dominates the induced electromagnetic methods. The skin depth permits the characterization of the investigation depth, which as can be seen increases according to the square root of the product of medium resistivity and period. Although it has been defined for homogenous media its use can be extended to heterogeneous cases as well (e.g. geologic structures).

The ratio E_x/H_y has the physical dimension of an electrical resistivity and defines a complex quantity called "impedance", which is a function of the electrical parameters of the subsoil. Thus, the impedance can be written as:

$$Z_{xy} = {E_x}\Big/{H_y} \quad (2.25)$$

and the resistivity of the homogeneous medium can be directly obtained as:

$$\rho = \frac{1}{\omega\mu}\left|Z_{zy}\right|^2 \quad (2.26)$$

2.4 THE MAGNETOTELLURIC TRANFER FUNCTION

In contrast to other geoelectrical methods, which are based on the study of the relationship between electromagnetic fields and their sources, the MT method is studying the ratios between the horizontal components of the electric (telluric) and magnetic fields to investigate the electrical conductivity structure of the Earth. A MT transfer function is defined as a function that relates the measured EM fields at a given frequency. It depends only on the electrical properties of the material the EM waves propagate through and not on the EM source. The most common MT transfer functions are represented by the impedance tensor Z or MT tensor and the geomagnetic transfer function (also known as the tipper vector or the vertical magnetic transfer function). Thus, estimating Z, it is possible to gain information about the distribution of the electric properties of the subsoil. Weaver et al, (2000) introduced the term magnetotelluric tensor, M (ω) (m/s), which uses $\vec{B}$ instead of $\vec{H}$ to define the relationships between the field components.

2.5 EARTH'S MT DIMENSIONALITY MODELS

The MT transfer functions and particularly the relationships between their components are reduced to specific expressions depending on the spatial distribution of the electrical conductivity being imaged. These spatial distributions, known as geoelectric dimensionality, can be classified as 1D, 2D or 3D (The complexity of the impedance tensor depends on the dimensionality of the subsurface medium. In the 1D and 2D case there are a few simplifications that become invalid once the complexity of the structure increases.)

1D model

For the simple case of a 1D, isotropic layered Earth, we consider a subsoil model in which the resistivity is a function of depth, that is $\rho = \rho(z)$. The equations found for the homogeneous half space still holds, but in this case it is not possible to directly obtain the resistivity ρ of the subsoil. For this reason a new quantity, the apparent resistivity ρa, can be introduced as the real resistivity of an ideal homogeneous and isotropic half space which, for each fixed frequency, gives a value on the Earth surface:

$$\rho_a(\omega) = \frac{1}{\omega\mu}|Z|^2 \quad \text{and} \quad \phi(\rho_a) = arctg\frac{\mathrm{Im}(Z)}{\mathrm{Re}(Z)} \qquad (1.27)$$

2D model

In a two-dimensional Earth, the conductivity is constant along one horizontal direction while changing both along the vertical and the other horizontal directions. The direction along which the conductivity is constant is known as geoelectrical strike or strike. So the resistivity is a function both of the depth z and of a direction between x and y. Let's assume that $\rho = \rho(x, z)$ and that the *y*-direction is the symmetry axis called "strike". In this case, any linear polarized electromagnetic wave can be decomposed into two waves, having respectively H and E parallel to the strike direction.

Therefore, Maxwell's equations can be written as:

- For E parallel to the strike direction we known that: $\vec{E}(0, E_y, 0), \vec{H}(H_x, 0, H_z)$, so

$$\frac{\partial H_x}{\partial z} - \frac{\partial H_z}{\partial x} = \frac{E_y}{\rho} \qquad (2.28)$$

$$-\frac{\partial E_y}{\partial z} = i\omega H_x \mu_0$$
$$\frac{\partial E_y}{\partial x} = i\omega H_z \mu_0 \qquad (2.29)$$

$$\frac{\partial H_x}{\partial x} + \frac{\partial H_z}{\partial z} = 0 \qquad (2.30)$$

- For H parallel to the strike direction we known that: E ⃗(E_x,0,E_z),H ⃗(0,H_y,0), so

$$-\frac{\partial H_y}{\partial z} = \frac{E_x}{\rho}$$
$$\frac{\partial H_y}{\partial x} = \frac{E_z}{\rho} \qquad (2.31)$$

$$\frac{\partial E_x}{\partial z} - \frac{\partial E_z}{\partial x} = i\omega H_y \mu_0 \qquad (2.32)$$

$$\frac{\partial E_x}{\partial x} + \frac{\partial E_z}{\partial z} = 0 \qquad (2.33)$$

Combining above equations, it results:

- E parallel to the strike direction:

$$-\frac{1}{i\omega\mu_0}\frac{\partial^2 E_y}{\partial z^2} - \frac{1}{i\omega\mu_0}\frac{\partial^2 E_y}{\partial x^2} = \frac{E_y}{\rho} \qquad (2.34)$$

- H parallel to the strike direction:

$$-\frac{\partial^2 H_y}{\partial z^2}\rho - \frac{\partial^2 H_y}{\partial x^2}\rho = i\omega H_y \mu_0 \qquad (2.35)$$

Solving this equations, on the Earth surface E and H components can be linked together according to:

$$. \begin{cases} E_x = Z_{xx}H_x + Z_{xy}H_y + Z_{xz}H_z \\ E_y = Z_{yx}H_x + Z_{yy}H_y + Z_{yz}H_z \\ E_z = Z_{zx}H_x + Z_{zy}H_y + Z_{zz}H_z \end{cases} \qquad (2.36)$$

where *Z* is the impedance tensor (Smirnov M. Yu. 2003)

Considering that the vertical electric field at the air-Earth interface is (per boundary condition) zero, in the last of the equation in 2.36, E_z can be considered equal to 0 and H_z can be expressed as a function of H_x and H_y.

When the fields are measured in a reference frame coinciding with the strike frame, equation 2.36 can be simplified in:

$$\begin{cases} E_x = Z_{xy}H_y \\ E_y = Z_{yx}H_x \end{cases} \quad (2.37)$$

or, in matrix notation, as:

$$\begin{pmatrix} E_x \\ E_y \end{pmatrix} = \begin{pmatrix} 0 & Z_{xy} \\ Z_{yx} & 0 \end{pmatrix} \begin{pmatrix} H_x \\ H_y \end{pmatrix} \quad (2.38)$$

3D model

Since Tikhonov's and Cagniard's times, the MT method has dramatically developed. Starting from the 1D case (in Tikhonov's and Cagniard's time) through 2D case (in the 70's), it has now become feasible to invert data with respect to a 3D Earth model. In other words the inversion in three dimensions is an actual and important topic of modern MT.

This is the most general type of geoelectrical structure. If the conductivity distribution varies with depth and in both lateral directions, the problem becomes 3D. In this case no rotation by any angle is able to result in an impedance tensor where the diagonal elements approach zero. Here, the resistivity changes along all the directions ($\rho = \rho(x, y, z)$). Also the decoupling into two separate modes, discussed above, is no longer valid. The 3D Earth requires the determination of a full impedance tensor with four complex elements for each frequency as given by:

$$\begin{pmatrix} E_x \\ E_y \end{pmatrix} = \begin{pmatrix} Z_{xy} & Z_{xy} \\ Z_{yx} & Z_{yy} \end{pmatrix} \begin{pmatrix} H_x \\ H_y \end{pmatrix} \quad (2.39)$$

2.6 MT INSTRUMENTS

A complete MT24/LF system includes:

- The Receiver
- The Power Supply Module with charger
- The BF magnetic sensors
- The Electrodes with dipole cables
- A GPS system
- A laptop computer
- And all other required cables and connectors.

The MT24/LF system

The MT24/LF system is a magnetotelluric receiver that uses a power efficient CPU and dual high and low speed 24-bit A/D acquisition. It employs CompactFlash memory for data storage and firmware. The combination of high accuracy oscillator along with GPS synchronization allows the unit to be used even in areas of dense forest coverage.

The simplicity of field operation makes the MT24/LF ideal for continuous conductivity imaging of the subsurface. Conductivity information is calculated from measurements of surface electric and magnetic fields along a profile line. MT24/LF obtains depths information at one site setup by measuring signals over a wide frequency range. The standard MT24/LF configuration records orthogonal electric and magnetic fields which are processed to provide tensor impedance measurements for interpreting complex 2D and 3D structures.

The MT24/LF Receiver (Fig. 2.5) accepts input from the sensors and performs amplification, filtering, power distribution, analog to digital (A/D) conversion and storage of time series. It interfaces with the portable system computer for acquisition configuration.

Figure 2.5: MT24/LF Receiver

The Receiver uses a 32-bit CMOS processor with very low power consumption. It has six CPU-controlled high speed 24-bit A/D for sampling at high frequency, and eight low speed 24-bit A/D for sampling at low frequency. This feature simplifies field operation by allowing simultaneous data collection in low and high frequency bands. The system uses one CompactFlash memory card for data storage. Packaging is made robust and compact through the use of Pelican Protector Case.

Magnetic Sensors

The sensors are EMI's BF magnetic feedback induction sensors mainly intended for use in geophysical explorations. The sensors are constructed using a high magnetic permeability, mu-metal core with proprietary windings. The coil windings are shielded and epoxy potted inside fiberglass housing. Each sensor includes a matched low noise preamplifier mounted at one end of the coil tube. The sensor is optimized to maximize noise performance for a given length/weight specification. There are currently four standard BF sensor designs, but the type recommended for the MT24/LF is the BF-4. The BF-4 Sensor is ideal for data collection in the band of 0.0001 Hz to 700 Hz.

Electrodes

The type of electrode to be used with the MT24/LF depends on the application. In our case, the type that it is used is 1 kHz and Pb-PbCl2 non-polarized electrodes with 100m cables

GPS Unit

The GPS unit is model GPS 35-LVS from Garmin. It is a complete 12- channel GPS receiver and embedded antenna that tracks up to twelve satellites at a time while providing one-second navigation updates and low power consumption. The GPS 35-LVS is housed in a black, water-resistant case designed to withstand rugged operating conditions. It has an attached 10-foot power/data cable with a 7-pin Tajimi connector. The system communicates via two RS232 compatible bi-directional communication channels. Internal memory backup allows the unit to retain critical data such as satellite orbital parameters, last position, date, and time.

CHAPTER III: RESULTS, PROCESSING, ANALYSIS

3.1 THE MT-STATION OF OMALOS (CRETE, GREECE)

The Mt station installed in Omalos contains:

- a MT24LF receiver
- external GPS
- three BF Magnetic Field Induction Sensors to measure the N-S, E-W and the vertical component of the magnetic field
- two 100m dipole lines with Pb-$PbCl_2$ non-polarized electrodes to measure the N-S, E-W of the electric field
- CompactFlash memory card for data storage.

The station has been heavily modified in order to make it a continuous unmanned operating system with long-time autonomy, full remote control and telemetry. To do that, the crucial point was the necessity of uninterruptible power that could be avoided with the exploitation of the solar energy (renewable energy) because as we know, Crete is characterized by a great average of daily sunny hours (8.67) and more than 300 days of sunshine per year providing the station with energy autonomy.

In addition to the standard component above mentioned, the MT station has been provided with:

- Solar Panel 12V/95W combined with a battery of 60AH for energy storage.
- 3G Router for wireless internet access through mobile network
- Low Power Field Computer (netbook type)
- System Controller based on MSP430F5438A Microcontroller

The solar panel was selected appropriately so that in a sunny day close to the aforementioned average could fully charge the battery which in turn is able to power the whole MT-station for about 10 days without any sunshine.
The System Controller (Kalisperi et al., 2013) stands for the “remote master control” of the MT-station. It checks all the units of the station and provides the variety of the necessary constant and

stable power voltages. Furthermore, the System Controller is equipped with a GSM module in order to accept remote commands from a distant user. Finally, the System Controller checks and records all the vital parameters and status of the permanent MT-station, i.e., charge current, system current, battery voltage, laptop status, MT24LF Status, 3G router status and all this information is available to distant user through GSM.

3.2 THE MT-STATION OF TRAMUTOLA (AGRI VALLEY,ITALY)

The Mt station installed in Tramutola contains:

- a MT24LF receiver
- external GPS
- three BF Magnetic Field Induction Sensors to measure the N-S, E-W and the vertical component of the magnetic field
- three 50m dipole lines with Pb-$PbCl_2$ non-polarized electrodes to measure the N-S, E-W (W-E, redundant) of the electric field
- CompactFlash memory card for data storage.

The station has been equipped with high capacity batteries that guarantee up to 2 months of autonomy. Data retrieving is manual and it is usually done on a monthly basis.

3.3 DATA ACQUISITION

The acquisition of MT data involves the recording of the time variations of the natural electric and magnetic fields simultaneously. In the logistically ideal case, both horizontal and the vertical magnetic fields are recorded, but if necessary one can omit the vertical component. For the electric field only the two horizontal components are recorded. In the first place, setting up a vertical electrical dipole is logistically very expensive (or impossible), but the main reason is that the vertical electric field at the air-Earth interface is (per boundary condition) zero.

The ideal location for recording MT data is far from human interference, far from electrical noise (e.g., DC train lines, electric fences, power lines and mining activity) and in an area with minimal topography, that allows equipment protection (i.e., soft soil that allows the burying of all sensors and cables, but also has a shady spot for the recording unit to protect it from the sun and overheating). As described in the previous chapter, both Omalos and Agri Valley sites have been chosen in order to have similar characteristics to the one of the ideal MT location.

3.4 DATA PROCESSING: FROM TIME-SERIES TO TRANSFER FUNCTIONS

In what is following, it will be illustrated the steps that yield the impedance tensor (or MT transfer function) estimates from the acquired time series.

The Earth is regarded as a linear system that responds to an input process (e.g., a time-varying magnetic field) via a predictable output process, (e.g., a time-varying electric field).

The tranfer function is the ratio of these processes and because the systen is linear , the tranfer function does not depend on the amplitude of the input process. The estimation of the transfer functions can be hindered by noise in the input and output process: e.g., electric and magnetic fields which are not naturally induced but are rather associated with our technical civilisation. If the noise level is low, or the noise has a Gaussian distribution (the frequency of occurrence, plotted as function of the size of the noise, delinates a Gaussian bell), then a least-square estimation (in which the squared residuum, which is ot explained by the linear system , is minimised) is sufficient. Otherwise, the occurrence of outliers might force us to apply a 'robust' processing scheme. Most robust processing schemes operate in an iterative manner and use some measure of the departure of an individual contribution from the average to down-weight outliers in the next iteration. After electric and magnetic time series are collected, impedance tensor estimates for each site are made for discrete, evenly spaced frequencies. Processing of the time series to yield impedance tensor estimates is referred to as data processing, and MT responses (impedances or apparent resistivities) output from the data processing are typically referred to as MT data, since this is the quantity fit by forward and inverse models.

The digital time series collected during an MT survey can easily total a few Gigabytes; in contrast, the transfer functions of one site are a very small dataset, typically described by the complex impedance tensor at 30-50 evaluation frequencies. Several major advancements in magnetotelluric data processing have occurred in the past 20 years; Jones et al. (1989) describe some of the methods of deriving transfer function estimates. All these processing schemes

involve the following steps (in one way or another):i) preconditioning of the data, ii) conversion from the time to frequency domain and iii) estimation of the transfer functions.

Pre-conditioning is done to reduce the effects of trends and to remove severe noise (spikes). Also part of pre-conditioning is the splitting of the time series into segments of different length, depending on the period being calculated. The statistical result will be the better the more segments are used. Conversion from the time to frequency domain by means of a Fourier transformation of the data is needed because time series simultaneously contain information about many periods and therefore about many penetration depths. The estimation of the transfer functions phase, core of the MT data process, represents the step during which the previously obtained information is used to evaluate the MT transfer functions at some fixed frequencies.

3.5 ESTIMATION OF THE MT TRANSFER FUNCTION

The general equation that allows us the estimation of the MT transfer function is the equation 2.39 (see Earth MT Dimensionality Models paragraph) which links, in the most general case, the acquired components of the electric and magnetic fields (E_x, E_y and H_x, H_y respectively) to the impedance tensor Z. Using the L^2 norm, in absence of noise, the best Z estimates will be the ones which, for each evaluation frequency, minimize the two functions derived from the equation 2.39:

$$\Psi = \sum_{i=1}^{N} (E_{x,i} - Z_{xx}H_{x,i} - Z_{xy}H_{y,i})(E_{x,i} - Z^{*}_{xx}H^{*}_{x,i} - Z^{*}_{xy}H^{*}_{y,i})$$

$$\Phi = \sum_{i=1}^{N} (E_{y,i} - Z_{yx}H_{x,i} - Z_{yy}H_{y,i})(E_{y,i} - Z^{*}_{yx}H^{*}_{x,i} - Z^{*}_{yy}H^{*}_{y,i}) \qquad (3.1)$$

Then it is needed to set $\frac{\partial \Phi}{\partial Z}$ and $\frac{\partial \Psi}{\partial Z}$ = 0, so the above equations can be minimized. Hence, for example the equations below can be obtained from which the elements of Z can be derived:

$$Z_{xx} = \frac{\langle E_x, H^{*}_x \rangle \langle H_y, H^{*}_y \rangle - \langle E_x, H^{*}_y \rangle \langle H_y, H^{*}_x \rangle}{\langle H_x, H^{*}_x \rangle \langle H_y, H^{*}_y \rangle - \langle H_x, H^{*}_y \rangle \langle H_y, H^{*}_x \rangle}$$

$$Z_{xy} = \frac{\langle E_x, H^{*}_y \rangle \langle H_x, H^{*}_x \rangle - \langle E_x, H^{*}_x \rangle \langle H_x, H^{*}_y \rangle}{\langle H_x, H^{*}_x \rangle \langle H_y, H^{*}_y \rangle - \langle H_x, H^{*}_y \rangle \langle H_y, H^{*}_x \rangle}$$

$$Z_{yx} = \frac{\langle E_y, H^{*}_x \rangle \langle H_y, H^{*}_y \rangle - \langle E_y, H^{*}_y \rangle \langle H_y, H^{*}_x \rangle}{\langle H_x, H^{*}_x \rangle \langle H_y, H^{*}_y \rangle - \langle H_x, H^{*}_y \rangle \langle H_y, H^{*}_x \rangle}$$

$$Z_{yy} = \frac{\langle E_y, H^{*}_y \rangle \langle H_x, H^{*}_x \rangle - \langle E_y, H^{*}_x \rangle \langle H_x, H^{*}_y \rangle}{\langle H_x, H^{*}_x \rangle \langle H_y, H^{*}_y \rangle - \langle H_x, H^{*}_y \rangle \langle H_y, H^{*}_x \rangle} \qquad (3.2)$$

Quantities such as $\langle A_k , A_k^* \rangle$, with k=x or k=y, are defined auto-powers and represent the product of one of the components of the electric/magnetic field for its complex conjugate (eq. 3.3)

$$\langle A_k , A_k^* \rangle^{1/2} = \sqrt{\frac{1}{n}\sum_{i=1}^{n} A_k A_k^*} \qquad (3.3)$$

Quantities $\langle A_k , A_j^* \rangle$ with k=x,y, j=x,j and k≠j or $\langle A_k , B_k^* \rangle$ are, on the other hand, defined cross-powers because they are the product of different components of the same field or the product of components of different fields.

In actual cases, nevertheless, noise has to be taken into account. Any measured signal can be thought as the sum of two contributions coming from the signal that we want to record and from the noise. The auto-powers are the sum of the signal and noise power, while the cross-powers will be affected by noise presence only if it is coherent among the different signals. Consequently, noise presence will yield to underestimate or to overestimate the impedance tensor elements.

The failure of the LS impedance tensor estimate can be traced to two fundamental inadequacies of the simple model of equation 3.1.

The linear statistical model is appropriate to the case where noise is restricted to the output or "predicted" electric field channels, while the input magnetic fields are observed without error. The violation of this assumption would result in the downward bias of estimated impedance tensor amplitudes. To avoid these bias errors the remote reference (RR) method, in which horizontal magnetic fields are recorded simultaneously at a second (remote) site and correlated with the EM fields at the local site. The RR MT impedance estimates are often substantially improved (less biased and more stable) over those obtained using the single station LS approach.

The simple LS estimator implicitly assumes a Gaussian distribution for the errors in equation (3.1). This assumption often fails for MT data because of the nonstationarity of both signal and noise.

Several MT processing methods have been proposed that attempt to exploit the above facts by adaptive screening or weighting of the data. Recently, the regression M-estimate (RME) (c.f., Huber, 1981) has been adapted to yield impedance estimates that are robust to violations of

distributional assumptions and resistant to outliers (Egbert and Booker, 1986; Chave and Thomson, 1989; Chave et al., 1987; Larsen, 1989; Sutarno and Vozoff, 1991).

Hence, it is crucial to adopt an estimation technique able to minimize noise effects, which in this thesis was the Robust Remote Reference Method.

3.6 REMOTE REFERENCE

The remoter reference method as introduced to magnetotellurics by Goubau et al. [1978] and developed by Gamble et al [1979]. It is based on classical principles but utilizes additional observations of the electromagnetic field at a site some distance from the station of interest to reduce the influence of noise. This is done because, unlike noise, the signal, having regard to the source that generates it, appears to be uniform over scale larger than those related to the noise. The necessary separation of the two measurements depends on the local geology, the source field behavior and the instrument noise.

It is instructive to consider the remote reference method in the context of norm minimization used earlier. Let the local electric (E) and magnetic (H) fields and the remote magnetic (R) field be observed over the same time interval and processed into frequency domain data in an identical manner. At the first site, the response functions satisfy equation 2.39 that can be rewritten as:

$$E = HZ + \delta \quad (3.4)$$

While at the second site a similar relationship is

$$\mathrm{E} = \mathrm{R}(Z + \delta z) + \delta_R \quad (3.5)$$

with the terms "δ" and "δ_R" indicating the possible noise presence and with the term δz accounts for any changes in the response function using the remote magnetic field caused by the separation of the electric and magnetic field measurements.

As for equation 3.1, the remote reference response functions are computed by minimizing the residuals, yielding to:

$$
\begin{aligned}
Z_{xx} &= \frac{\langle E_x, R^*_x \rangle \langle H_y, R^*_y \rangle - \langle E_x, R^*_y \rangle \langle H_y, R^*_x \rangle}{\langle H_x, R^*_x \rangle \langle H_y, R^*_y \rangle - \langle H_x, R^*_y \rangle \langle H_y, R^*_x \rangle} \\
Z_{xy} &= \frac{\langle E_x, R^*_y \rangle \langle H_x, R^*_x \rangle - \langle E_x, R^*_x \rangle \langle H_x, R^*_y \rangle}{\langle H_x, R^*_x \rangle \langle H_y, R^*_y \rangle - \langle H_x, R^*_y \rangle \langle H_y, R^*_x \rangle} \\
Z_{yx} &= \frac{\langle E_y, R^*_x \rangle \langle H_y, R^*_y \rangle - \langle E_y, R^*_y \rangle \langle H_y, R^*_x \rangle}{\langle H_x, R^*_x \rangle \langle H_y, R^*_y \rangle - \langle H_x, R^*_y \rangle \langle H_y, R^*_x \rangle} \\
Z_{yy} &= \frac{\langle E_y, R^*_y \rangle \langle H_x, R^*_x \rangle - \langle E_y, R^*_x \rangle \langle H_x, R^*_y \rangle}{\langle H_x, R^*_x \rangle \langle H_y, R^*_y \rangle - \langle H_x, R^*_y \rangle \langle H_y, R^*_x \rangle}
\end{aligned}
\tag{3.6}
$$

which is the remote reference response function given by Gamble et al. [1979].

The advantages of the remote reference method are well-known. Since the cross powers of H and R appear in the denominator of eq. 3.6 rather than the auto power of H , remote reference estimates are in principle not biased downward by noise in the local magnetic field H (given that the two noise in the local and remote magnetic channels should not be correlated). The remote reference method effectively eliminates this bias if the noise is not correlated between the two sites. It also has some effect in reducing local electric field noise if it is uncorrelated with the remote magnetic field. However, the remote reference method is not robust; if there is correlated noise on all of the channels, then it will break down like least squares. Such noise is obviously not instrumental but must be related to inhomogeneous source structure. It should also be noted that the remote reference method is not data adaptive since there is no explicit weighting based on data quality, so that severe contamination of the electromagnetic field at one of the sites cannot necessarily be removed.

3.7 EGBERT'S ROBUST PROCESSING

The current state-of-the-art method for data processing is the EMTF program: a robust single and multiple-station processing routine by Egbert [1997; 2002]. The term robust comes from the robustness of the method to a certain percentage of noise or bad data in the MT time series. The program is based on the use of a hybrid norm.

The RME (regression M-estimate), introduced by Huber et al. (1981) and additional elaborated by Egbert and Booker (1986), Chave et al. (1987), Chave and Thomson (1989), can be applied to all the data characterized by a predominantly Gaussian distribution and it is based on the use of the L2 norm, when the residuals are small, and on the use of the L1 norm for large residuals. E.g., for the x component of the electric field, the following quantity has to be minimized:

$$\sum_{i=1}^{n} w_i \left| \frac{E_{x,i} - (Z_{xx} H_{x,i} + Z_{xy} H_{y,i})}{\sigma} \right|^2 \qquad (3.7)$$

where the w_i weights are calculated from the data itself by an iterative process whose starting point are the residuals estimated using L_2. Based on the values of these residuals, a first determination of the w_i weight is obtained and used to minimize eq. 3.7; the new residuals lead to a new determination of the weight and so on.

In the RME method the used weights are those introduced by Huber (1981) :

$$w_i = \begin{cases} 1 & \text{if} \quad r_i \le 1.5 \\ 1.5/r_i & \text{if} \quad r_i > 1.5 \end{cases} \qquad (3.8)$$

with

$$r_i = \left[\frac{E_{x,i} - (Z_{xx} H_{x,i} + Z_{xy} H_{y,i})}{\sigma} \right] \qquad (3.9)$$

In what follow, an overview of the EMTF program is given.

Overview of EMTF

The use of the transfer function (TF) estimation programs in EMTF can be decomposed into three dinstict steps. These are:

1. Reformat the data: In general data files come in lots of different formats, so making a general package of processing software which accomodates all possibilities is difficult. It is hence necessary to reformat the input data according to a standard format.
2. Window and fourier tranform data segments: Input to this program is a data file in either the “standard binary” or simple ASCII forms, a file describing system parameters, several files which control program options and (optionally) instructions about sections of data to omit from further processing. Output is a file consisting of Fourier coefficients (FCs) ordered by frequency. The output FC files are used by all subsequent frequency domain processing programs, including single station and remote reference tranfer function program tranmt and the multiple station program multmtrn.
3. Robust estimation of transfer functions: Input is the ordered Fourier coefficient file(s) and files controlling program options. The program can handle an arbitrary number of data channels. Output is a file containig TFs and full error covariances, from which all standard MT and GDS interpetation parameters can be computed in any specified coordinate system.

Windowing and Fourier Transforming Data Segments

The windowing and FFTing if data segments to produce the complex frequency domain data vectors for each station is accomplished by program dnff. The programs have been designed for Fourier transforming time series prior to array processing. To accommodate a range of instruments, sampling rates, etc., a lot of generality has been built into this program.
The input data file expected by this program should be is simple ASCII file containing the time acquire EM time series reformatted as described in the previous paragraph (Egbert and Eisel 1998)

There are (up to) four configuration files needed for a run. In summary these are:

i. decset.cfg controls the windowing and decimation options and decset.cfg is the default name.
ii. pwset.cfg is used to control pre-whitening options. A pri-prolate window is used for tapering the time series data before FFTing.
iii. data.sp is used to specify system parameters, including sampling rates, clock drift parameters, sensor orientations, electrode line lengths, instrument specific analogue filter corrections and factors for conversion of data from counts to physical units.
iv. dat.bad tells the program about "bad data". This file is optional. If it is not found the program prints a warning and proceeds under the assumption that there are no "bad data" segments. Data segments which are obviously contaminated by significant instrument malfunction, or other obvious problems, can be noted in this file so that they will be omitted from subsequent processing. In its current implementation, bad segments can be flagged with an integer 1, 2, 3, 4 and they are supposed to mean:

1) Magnetics bad.
2) Electrics bad.
3) Long period bad.
4) All bad.

The basic goal is to use data segments that are as short as possible, given the desired resolution in the frequency domain. We thus use short (e.g., 128 points) overlapping segments of the input time series to get Fourier coefficients for the highest possible frequencies. To get lower frequencies a longer time window is needed. To do this efficiently, the porgram digitally low pass filters the input series and then decimates the smoothed time series. This filtering and decimation process is repeated as often as desired (to produced levels 1, 2, 3, 4…).

Transfer Function Estimation Program

The tranfer function program (tranmt) computes robust single station and remote reference transfer functions between a pair of local reference channels (generally two orthogonal orizontal magnetic field components) and some number of other channels. As well there is an automatic “leverage cotrol” feature (e.g., Chave and Thomson, 1989) and an option to use a hybrid coherence sorting/regression M-estimate, as described by Egbert and Livelybrooks (Egbert G. D. and Livelybrooks D. W. 1996) Error bars are computed using the asymptotic approach edscribed in Egbert and Booker (1986).

The input expected by this program is one or more of the FC files output by dnff. It is possible to have FCs for local and remote sites in the same or different FC files.

In addition to FC files there are 3 required configuration files, plus one optional file, which are generically called tranmt.cfg, options.cfg and bs.cfg. Roughly, tranmt.cfg tells the program which data files to use, (and which “options” file to use), the options file options.cfg specifies processing options and the band setup file bs.cfg tells the program which frequency bands to compute TF estimates for. The optional configuration file ref.cfg is used to change default definitions of reference and predicted channels.

Currently tranmt outputs two files: A “Z-file” containing local TFs and error bars an d an opional file containing cross-spectra. All TFs are in the measurement coordinate system. The Z-files also contain channel information (orientations, channel names, etc.) and the full covarience of signal and residuals. With these matrices it is possible to correctly compute error bars in any coordinate system. The Z-files produced for single station, remote reference and multiple station processing are interchangeable. The results can be displayed using the Matlab program apresplt (Egbert G. D. 1998)

3.8 DATA ANALYSIS

The data analysed in this thesis are those acquired from both Omalos and Tramutola stations. In particular Omalos data were acquired during the first year of its operation (2012) when the station still was not permanent, hence the measurements were not continuous in contrast to the station of Tramutola.

For Omalos, the time series were registered through different bands, however in our case only L and J bands (Low frequency and High frequency domain) were processed, with a total duration of ten days. The data was separated in four folders:

1. Cre-01: With acquisition starting time in 19/5/2012 at 08:52:00 to 21/5/2012 at 00:35:00 for the L-band.
2. Cre-01-b: With acquisition starting time in 21/5/2012 at 08:32:00 to 24/5/2012 at 00:35:00 for the L-band.
3. Cre-01-c: With acquisition starting time in 24/5/2012 at 07:00:01 to 27/5/2012 at 00:35:00 for the L-band.
4. Cre-01-d: With acquisition starting time in 27/5/2012 at 07:00:00 to 30/5/2012 at 00:35:00 for the L-band.

The J-band was recorded for each day separately during the morning and the night for 25 minutes each.

For Tramutola, that the recording is continuous, the duration in total was 36 days. The time series were registered only for L and J bands. The data was divided in two files:

1. 2012_05_16: With acquisition starting time in 16/4/2012 at 10:43:56 to 22/5/2012 at 07:54:56 for the L-band and from 17/4/2012 at 01:00:00 to 01:59:59 for the J-band.
2. 2012_05_22: With acquisition starting time in 22/5/2012 at 08:19:12 to 18/6/2012 at 08:51:12 for the L-band and from 23/5/2012 at 01:00:00 to 01:59:59 for the J-band.

Before being processed with the Egbert's program, data have been reformatted, cleaned from the most evident noise effects and re-synchronized.

Reformatting the data

The time series for both sites were processed using the EMTF program. The sites were labeled as "Cre-01" (for Omalos) plus an identification letter for each folder (as seen above) and "Tr" (for Tramutola).

Before the processing, the data have been reformatted according to the Egbert's program requirements; every file corresponding to the above mentioned datasets (both J and L band) is a 6-columns ASCII-file in which each column contains data related to a specific channel recorded by the MT24LF system. As standard, odd columns (1, 3 and 5) contain data related to a magnetic channel (Hx, Hy or Hz) while even columns (2, 4, and 6) contain data related to an electric channel (Ex, Ey or Ez). In order to be used as input of the Egbert's code, the position of magnetic and electric channels in the data file has to be changed in order to have all the magnetic channels in the first columns. ASCII-files were hence transformed in the following way:

TRAMUTOLA

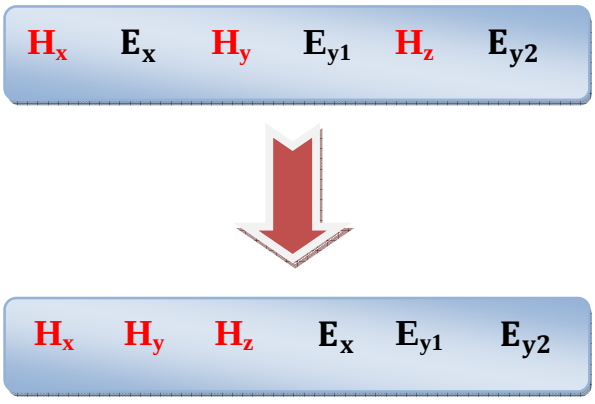

OMALOS

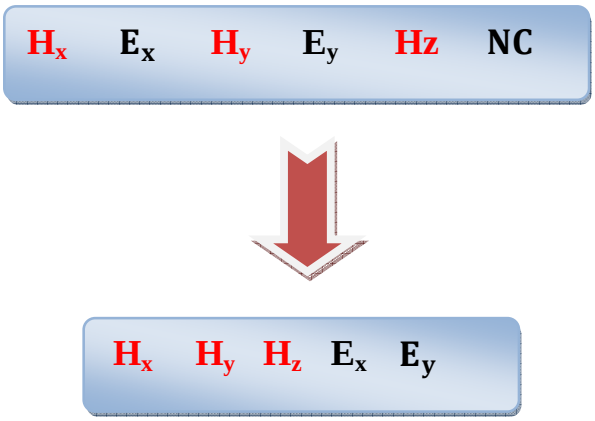

where NC stands for Not Connected.

Visual inspection of the time series: creation of the bad data file

One of the principal problems associated with the measurements themselves has been the impact of local electromagnetic noise. Any signals in measured electromagnetic fields corresponding to non-inductive or locally inductive sources can be considered to be noise. Additional sources of noise that lie external to the Earth are of three types:

i. Cultural
ii. Meteorological and
iii. Sensor

In populated areas, electricity power lines produce dominant 50 Hz and 150 Hz electromagnetic fields. Whilst noise at such frequencies is relatively easily eliminated by notch filtering, it can limit the dynamic range of magnetic induction coils and cause instrumental saturation. Power-line noise is highly polarized. Therefore, the effects of power-line noise are usually more

prevalent in one orthogonal measurement direction than in the other. Electricity generators can also produce significant levels of noise in the 50 Hz range. Electric field measurements are also susceptible to contamination from ground leakage currents arising from electric railways and electric fences, the noise spectra from which span broad frequency ranges making filtering difficult.

Automobiles represent a dual source of noise creating both magnetic and seismic disturbances, which generally can be negated by ensuring that the sensors are placed more than 20 m away from any road. Seismic vibration generates noise on the telluric components, creating problems between the electrodes and the ground.

The vibration of telluric lines in the wind can generate voltages comparable to short-period telluric signals. As a result of wind blowing on trees and bushes their roots may move within the Earth generating seismic noise, which may, in turn cause movement of the sensors and corresponding perturbations of the measured fields. Another source of meteorological noise is generated by local lightning discharges and also lightning may cause saturation of telluric amplifiers.

Sensor noise and noise arising from electronic circuitry is usually independent of signal power and random in nature, making it difficult to distinguish and harder to evaluate. However, sensor noise is generally low (e.g., less than 30 pT for a fluxgate magnetometer) for modern instrumentation.

At periods exceeding 1000 s, the signal-to-noise ratio is independent of signal power (Egbert and Booker, 1986), but at shorter periods, for which the power of the natural source field is more variable and contamination by cultural noise is more prevalent, signal-to-noise ratios can vary significantly. The presence of noise causes bias effects, including false depression or enhancement of calculated estimates.

In our attempt,to minimize as much as possible the noise caused of al the above factors, we modified slightly the Cre01l.dat file (only for the L-band), with the aim to eliminate all the parts of the time series, which could be considered as noise. Afterwards, we created the cre01l.bad file, with the discrimination of the bad segments mostly to be found in the magnetic channels and having a total number of 30 “noisy parts”.

Below (Fig. 3.1) it is shown the first part of the bad file with all kind of bad segments, except the integer 3 for long period bad data, which didn’t exist in our case.

File Edit Format View Help

30

600 2800 4

3500 4500 2

6500 6800 1

8300 9500 1

Fig 3.1: An example of the cre01l.bad file.

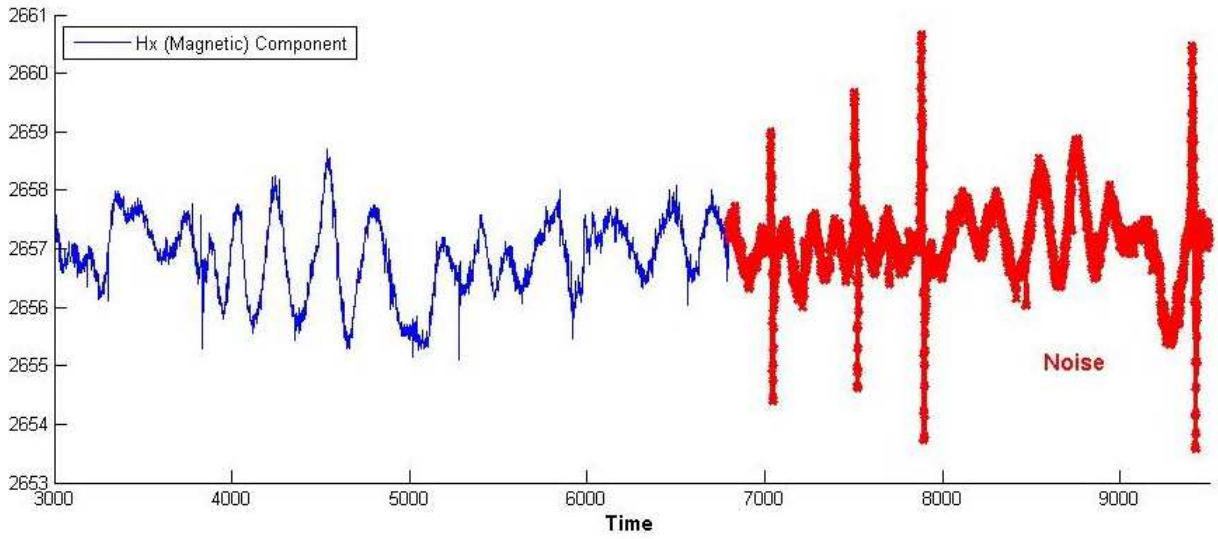

Figure 3.2: Noise recorded on the Hx (Magnetic) Component.

Figure 3.2 shows and example of magnetic data flagged as noisy in the bad data file; ranging between 7000 to 9500, the time series (Hx) is clearly affected by the presence of relevant spikes. Figure 3.3 shows and example of electric data flagged as noisy; from 0 to 3000, the signal (Ex) is characterized by random fluctuation with increased variance respect to the rest of the time series.

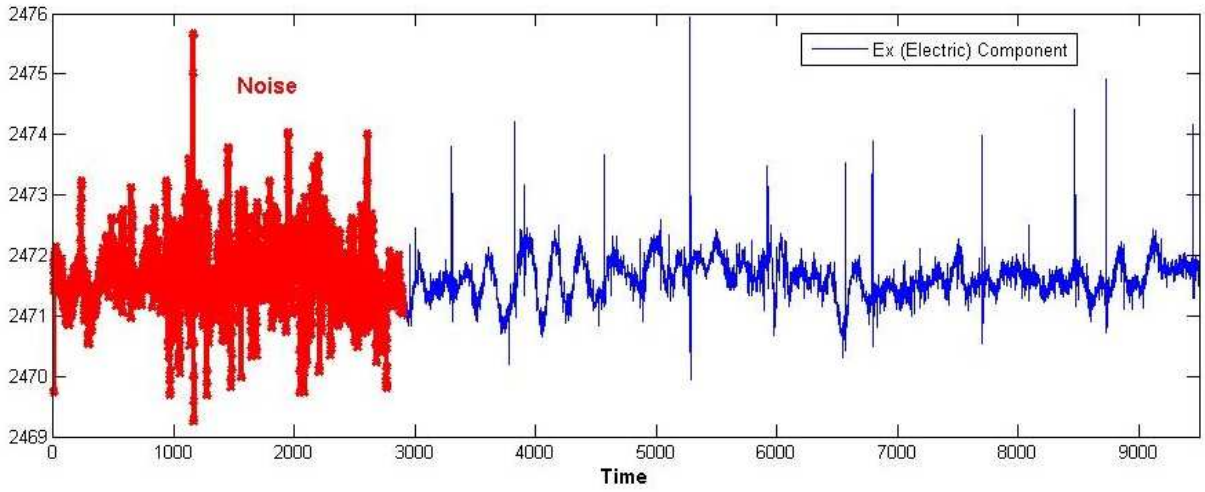

Fig3.3: Noise recorded on the Ex (Electric) Component.

Synchronization of the time series

In order to apply the remote reference between the two MT-stations, data coming from the remote and the local station has to be synchronized. Usually the synchronization is guarantee by the GPS module of the MT system. Unlucky, due to the fact that the station in Tramutola has a problem with the GPS drift, Omalos and Tramutola data can not be considered synchronized. This can be easily seen in Fig.3.4.

The two time series are characterized by the same trends but are visibly shifted one respect to the other of about a few seconds (15 seconds). For that very reason,we had to find a way to synchronize the signal based on a high level of precision and not only on the similarities of the shapes. Therefore, it was important to locate a characteristic that could be easily identified in both the time series.

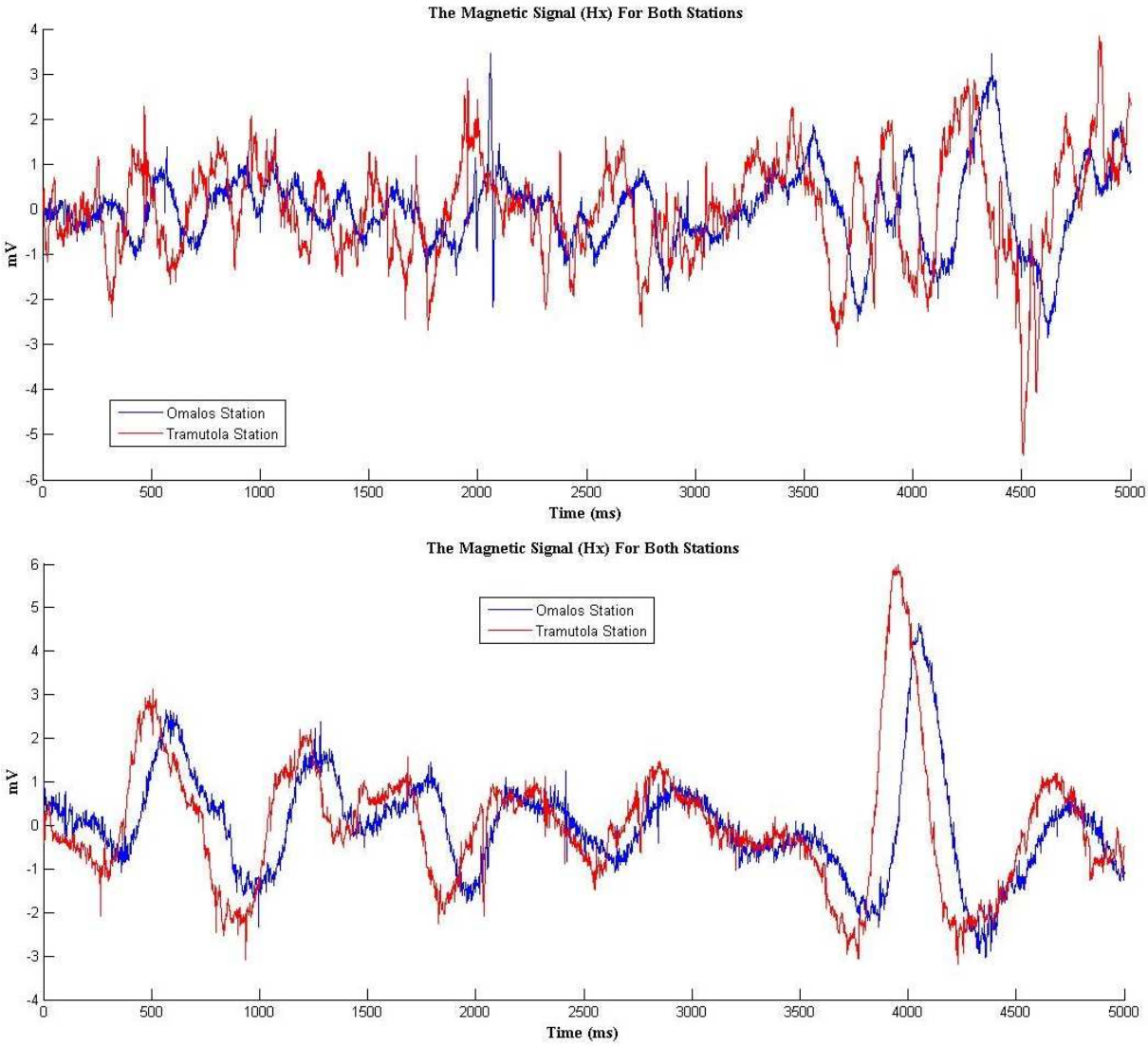

Fig. 3.4:The magnetic signal for both the MT-stations (Omalos and Tramutola), before the synchronization.

We noticed, that the magnetic channels are characterized by sets of spikes (one single scattered point), at least they can be considered spike at the 6.25 sampling frequency, that occur with the same time lag in both the local and the remote time series (Fig 3.5). Since they cannot be ascribed to a local disturbance of the signal due to their presence in both sites, we decided to use them to synchronize the time series.

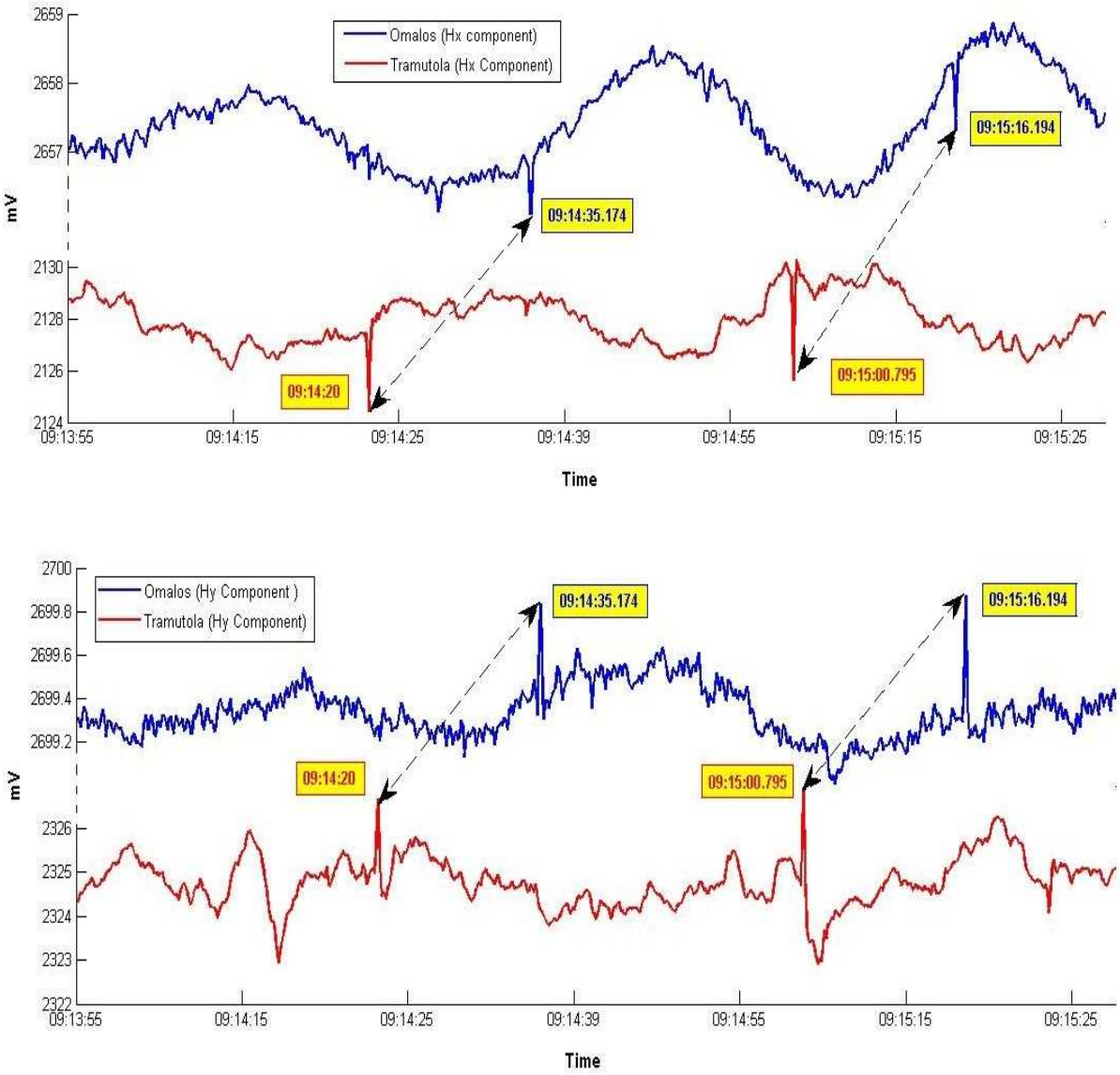

Fig 3.5: The two sets of spikes, found on both MT-stations, that were used to identify and ultimately to synchronize our signal between the local and the remote station (Omalos-Tramutola)

In order, to be able to use the above assumption, for the signal connected to the spikes, we had to execute the following steps:

1. Primarily, we found two sets of spikes on the magnetic channels (Hx, Hy) for the files of Cre01l.dat and Tr.dat that could be seen on both the time series of the stations.

The first set of spikes, for the Hx and Hy Components, was located at 09:14:35.174 for Omalos and at 09:14:20 for Tramutola. For the second set of spikes, the located time was at 09:15:16.194 for Omalos and at 09:15:00 for Tramutola, using the Asq.24 program. Each, located time had a specific number of points, which was related to the .dat file. So we had:

Station	**Spikes**	**Located time**	**Number of Points**	**Eliminated Points from the data**
Omalos	1^{st}	09:14:35.174	8469	17777931
Tramutola		09:14:20.395	17786400	
Omalos	2^{nd}	09:15:16.194	8727	
Tramutola		09:15:00.795	17786653	

Afterwards, we created a new file for Tramutola with exactly the same number of points that we found between Crete's and Tramutola's spikes, which was (as it is shown on the table) 17777931. The new file was named Tr_1.dat.

Lastly, the new data file (Tr_1.dat) was processed with Egbert's program. At first for the Single Station and then for the Remote Reference Method which, was what we wanted to accomplish.

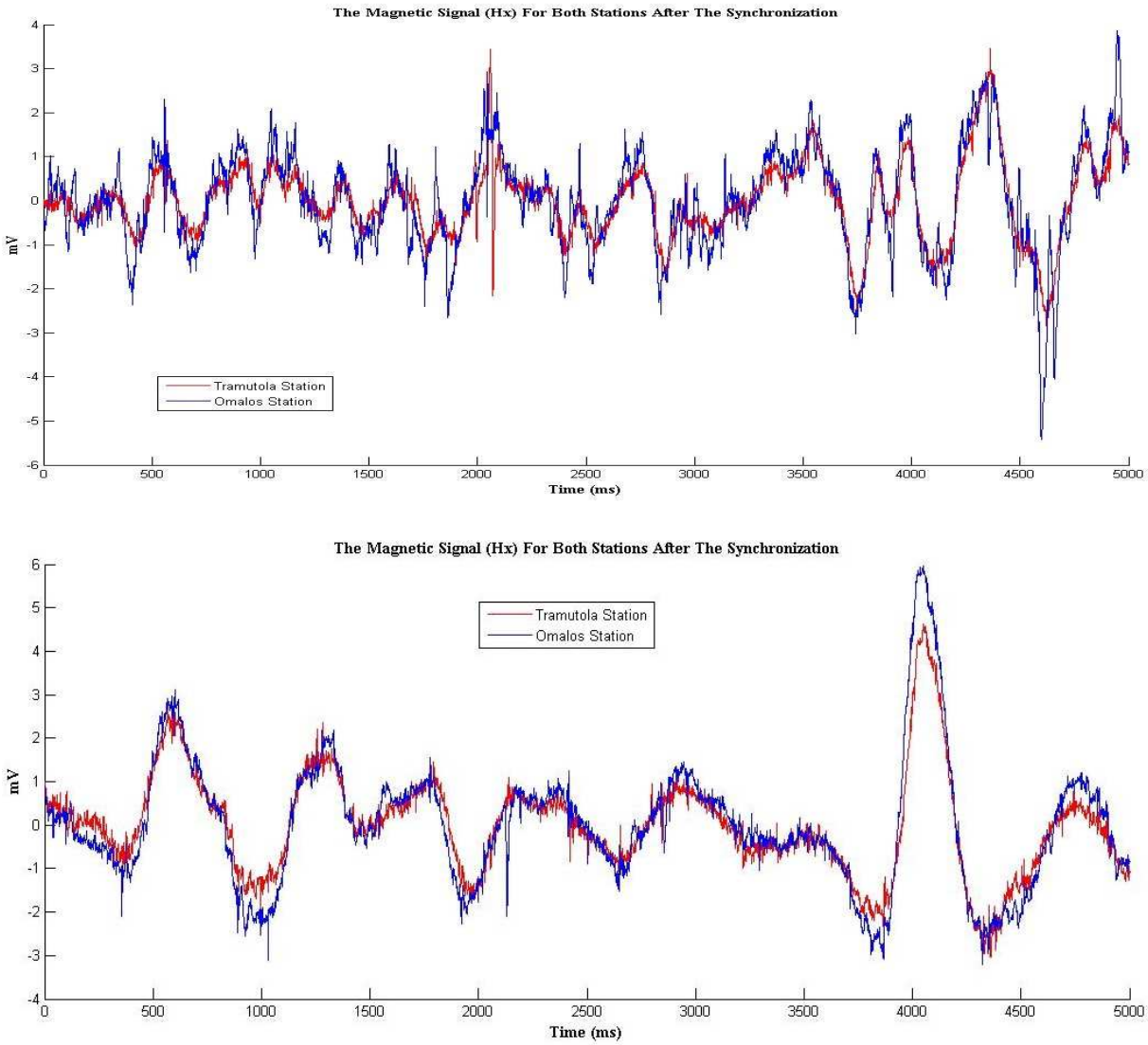

Fig3.6: The Magnetic Signal for both the MT-stations (Omalos and Tramutola), after the synchronization.

As, we can see in the Fig. 3.6 the synchronization was especially successful. The two signals, Omalos and Tramutola time series, look very similar, a fundamental prerequisite for the Remote Reference Method to be applied successfully.

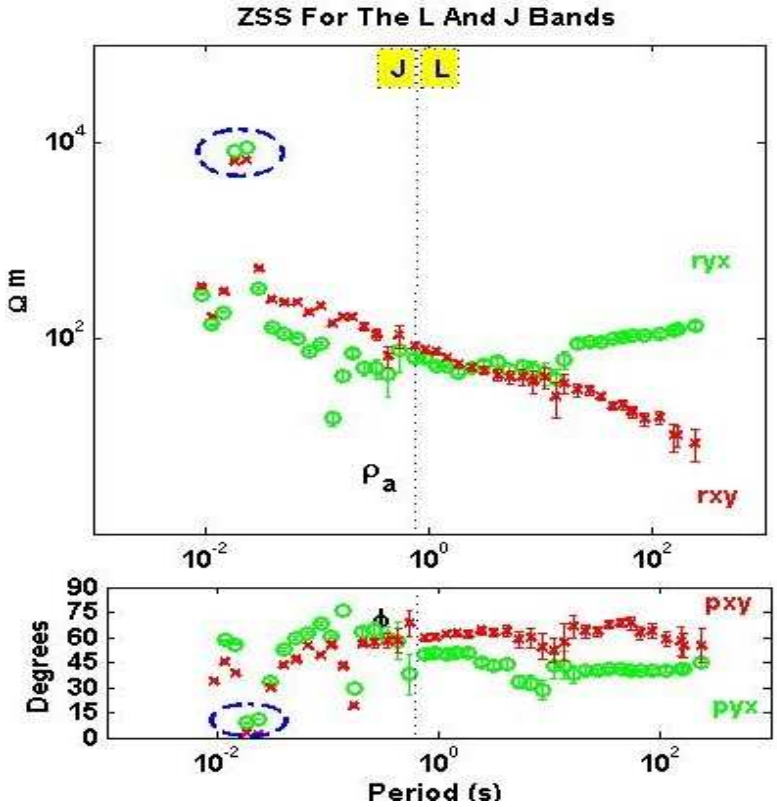

Figure 3.7: result of the Single Station analysis for Cre-01 (Cre01dl + Cre01dj1481204 Bands) data. Upper panel: apparent resistivity curves as a function of the sounding period. The two different sets of curves are related to different component of the impedance tensor Z; in particular the green curves to Zxy and the red curves to Zyx.

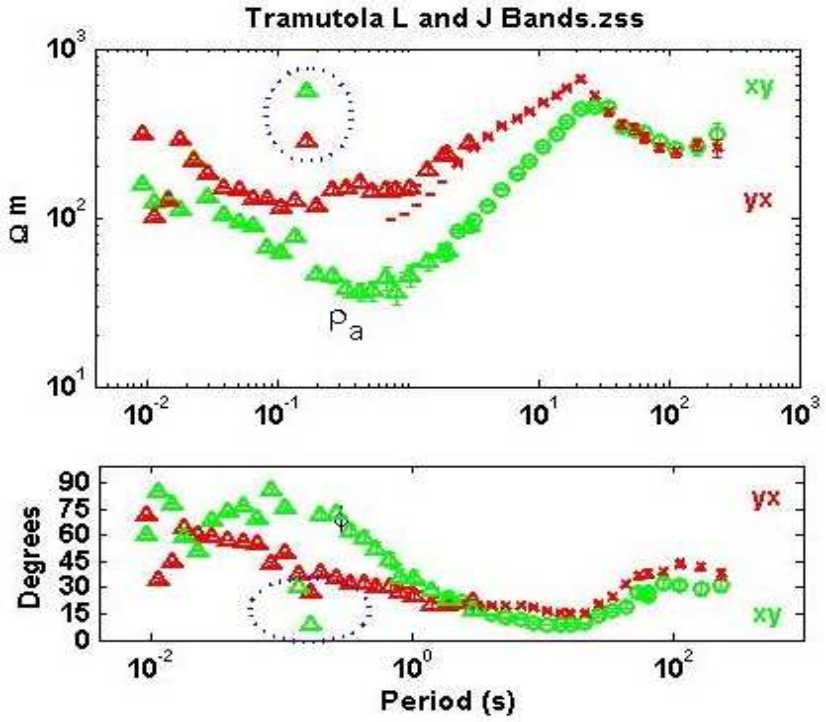

Figure 3.8: result of the Single Station analysis for Tr (L + J Band) data. Upper panel: apparent resistivity curves as a function of the sounding period. The two different sets of curves are related to different component of the impedance tensor Z; in particular the green curves to Zxy and the red curves to Zyx

Remote Reference Results for Tramutola

.

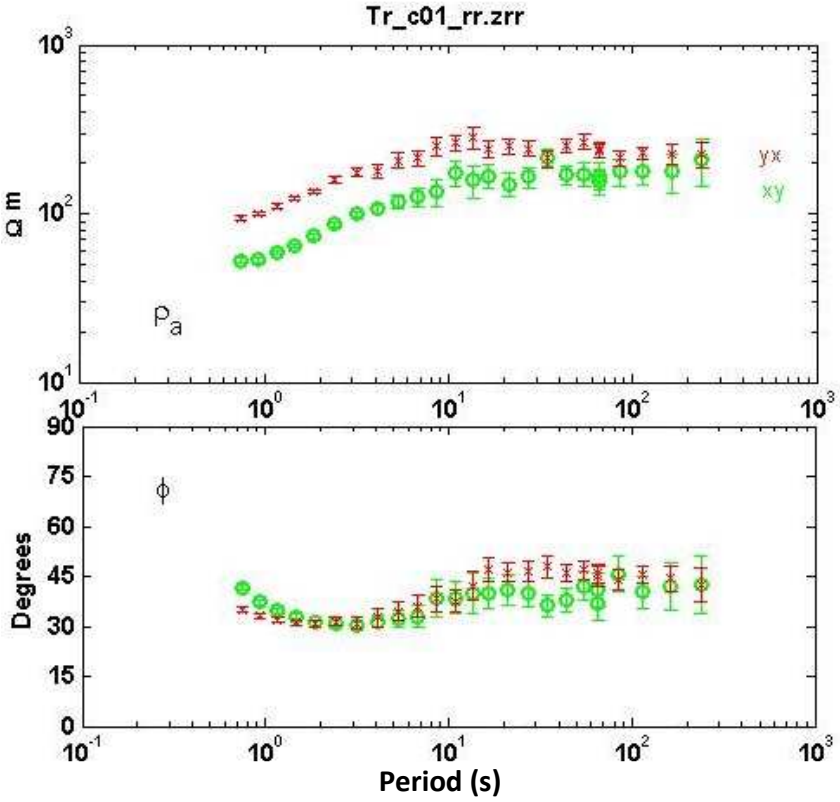

Figure 3.9: RR apparent resistivity and phases curves for Tramutola.

Remote Reference Results for Omalos

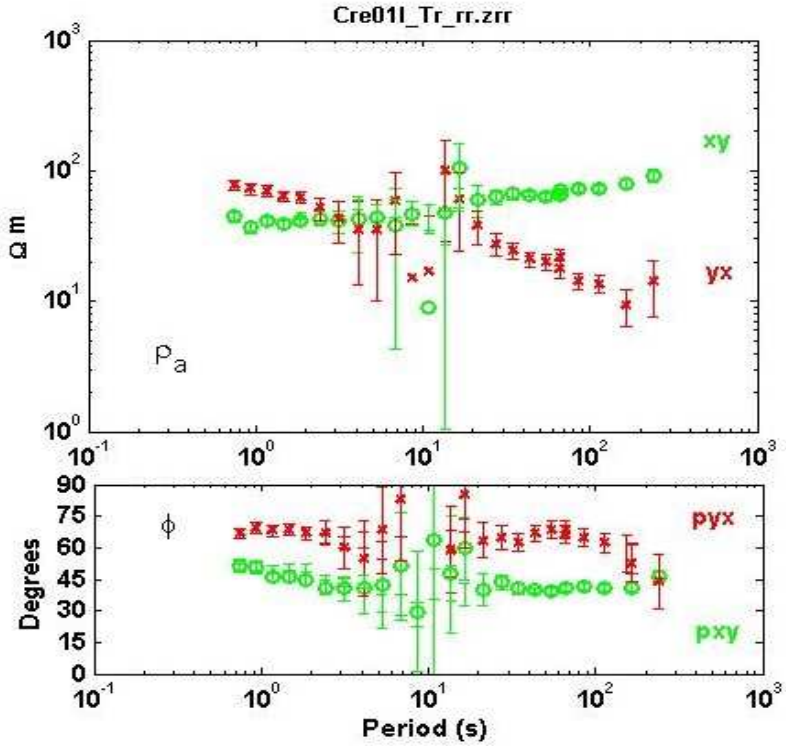

Figure 3.10: RR apparent resistivity and phases curves for Omalos

3.9 BOSTICK TRANSFORM

Resistivity curves-Skin depth using the Bostick transform

To highlight the importance of obtaining the most reliable MT results, the single station and the remote reference curves obtained for Tramutola will be used to infer a resistivity profile by using the simplest 1D inversion of the data: the Bostick transform.

Plane wave fields at the surface diffuse into the ground attenuating exponentially with depth. Low frequencies penetrate more deeply than high frequencies, the so-called skin-depth effect. The depth at which a plane wave is attenuated to 1/e of its value at the surface is the skin-depth, δ. In a layered half-space, the resistivity obtained for ρ_A is roughly equal to the average resistivity of layers down to the skin-depth.

The apparent resistivity vs. frequency data is called a magnetotelluric sounding. At the most fundamental level, interpretation of MT consists in finding the conductivity distribution vs. depth which matches the observed data. The available spectrum of natural fields from 10^{-4} to 10^{3} Hz yields depths of investigation from a few tens of meters to a few tens of kilometers in typical geologic sections.

A new presentation for magnetotelluric data was proposed to be used together with the traditional representation by Goldberg and Rotstein (1982). The result is an approximate depth-resistivity diagram which contains an indication of the data quality as well as the homogeneity of the subsurface. The new diagram is based on an immediate transformation of apparent resistivity and phase data and presentation of an approximate resistivity and depth data. Specifically, this transformation is based on the simple asymptotic expressions introduced by Bostick (1977):

$$\rho(D) = \rho_a(\omega)\left(\frac{\pi}{2\phi} - 1\right) \quad (3.10)$$

and

$$D = (\rho_a(\omega)/\mu\omega)^{1/2} \quad (3.11)$$

Where D is the depth, ρ (D) is the resistivity at depth D, ω is the frequency, $\rho_a(\omega)$ is the apparent resistivity at frequency ω, μ is the magnetic permeability, and ϕ is the phase. With expressions (3.10) and (3.11) both approximate resistivity and depth can be easily determined. The technique is applied to the raw apparent resistivity and phase data so that each apparent resistivity data point together with the corresponding phase data point is transferred into a data point in a resistivity-depth diagram.

The use of the Bostick (1977) inversion has acquired immediate popularity in geophysical service companies because of its simplicity. However, the usual procedure is to use it for the inversion of smoothed apparent resistivity curves and not for the separate data points. Thus, it is used only as an inversion routine and no use is made of its advantages in the presentation of the field data.

The result of this transformation applied to L-band Tramutola curves **is** shown in fig. 3.11

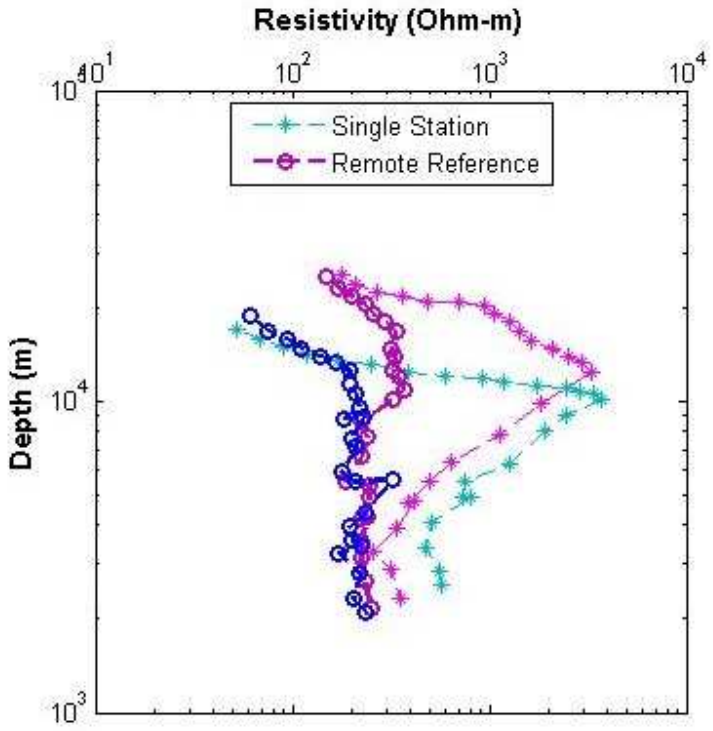

Figure 3.11: Resistivity curves-Skin depth using the Bostick transform. The "*" symbol indicates the Resistivity curves-Skin depth obtained from the single station MT curves. The "O" symbol indicates the Resistivity curves-Skin depth obtained from the Remote Reference MT curves. Blue and cyan curves are related to the xy component; Magenta and violet curves to the yx component.

CHAPTER IV: INTERPTATION, DISCUSSION

Most of the efforts in this thesis were focused on the analysis of the data coming from the two monitoring station of Omalos (Cre-01) and Tramutola (Tr). In the appendix A, additional data related to two more additional data sets (MT-surveys Cre-02 and Cre-03) will be presented.
Considering the sampling frequencies (500 Hz for the J band and 6.25 Hz for the L band), the application of the Robust Transfer Function Estimation Program described in Egbert, 1997, to our MT data allows to obtain resistivity and phase estimates in the sounding period range [0.0093s, 238 s].
Avoiding any discussion about the dimensionality of the data, it will be shown apparent resistivity and phases curves related to the off-diagonal components of impedance tensor Zxy and Zyx in the acquisition framework:.ie N-S, E-W.

Single station

After removing the bad data from the time series, robust Single Station (SS) processing was performed on the data. The outputs for the J+L band for Tr and Cre-01 are shown respectively in fig. 3.7 and 3.8.
Cre-01 curves are characterized by almost smooth trends. As common the short period range estimates (J band) are more disturbed than long period estimates (L band) as proved by the presence of scattered estimates.
The difference between the two components (green and red curves) over the whole sounding period range can indicate or a complex resistivity structure of the subsoil or a strike direction different from the acquisition framework one.
Estimates clearly suffer for the effects of EM cultural noise most probably connected to the presence of power line in the proximity of Omalos MT monitoring station. This can be testified by the two scattered estimates, highlighted by a blue dashed circle in fig. 3.7, at sounding period around 0.019 s, a period really close to the one characteristic of the power lines (0.02 s).
Tr curves are characterized by almost smooth trends. Also in this case, apart for long periods, the subsoil structure seems to be complex.

The effects of power line presence, even if less strong than in Cre-01, are still present as testified by the worsening of the estimates approaching 0.02s.
An anomalous pattern can be observed around 20 s where a cusp is present on the ρ_{yx} curve.

Remote Reference

The main focus in this thesis is the application of the Remote Reference method between the two permanent MT-stations in Greece (Omalos) and in Italy (Tramutola) with the distance to be around 905.08 km (fig. 4.1). Therefore, our target is the improvement of MT estimates quality and to try to asses which one between the two monitored sites can be considered as the quiet site (lower cultural noise presence).
The RR method was applied only for the L band (6.25 Hz sampling frequency) since it performs better in obtaining long sounding periods estimates. Only the magnetic fields have been used as remote fields.

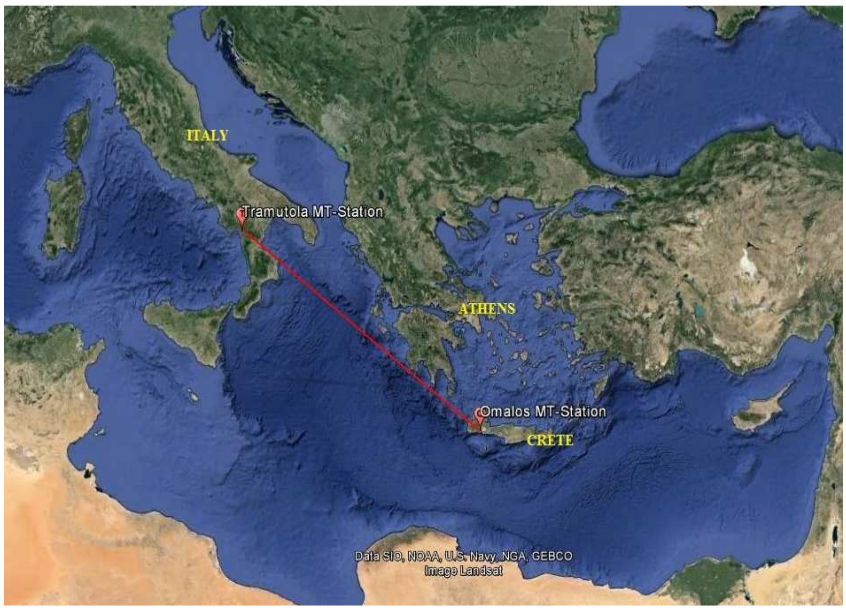

Figure 4.1: map showing the position of the two monitoring sites: Tramutola and Omalos.

Figure 3.9 shows the results of the RR for Tramutola using Omalos as remote. As it is possible to see, the curves are characterized by almost smooth trends. Furthermore it has to be noticed that slightly bigger error bars characterize the RR than the SS curves. This result is in agreement with the result of Jones at al. 1998:<<it should be noted that remote reference methods are not as efficient as single-station methods in that for a given length data set, remote reference results will always have larger associated statistical errors than standard LS ones.>>

The main difference between remote reference and single station curves can be better appreciated in fig. 4.2 where both the curves are plotted. The use of the remote reference techniques, in this case, allows to correct Tr and improve the reliability of the curves especially around 20 s where the cusp is no more present. Generally speaking the between 3s and 60 s, the RR method strongly modifies the shape of the MT curves.

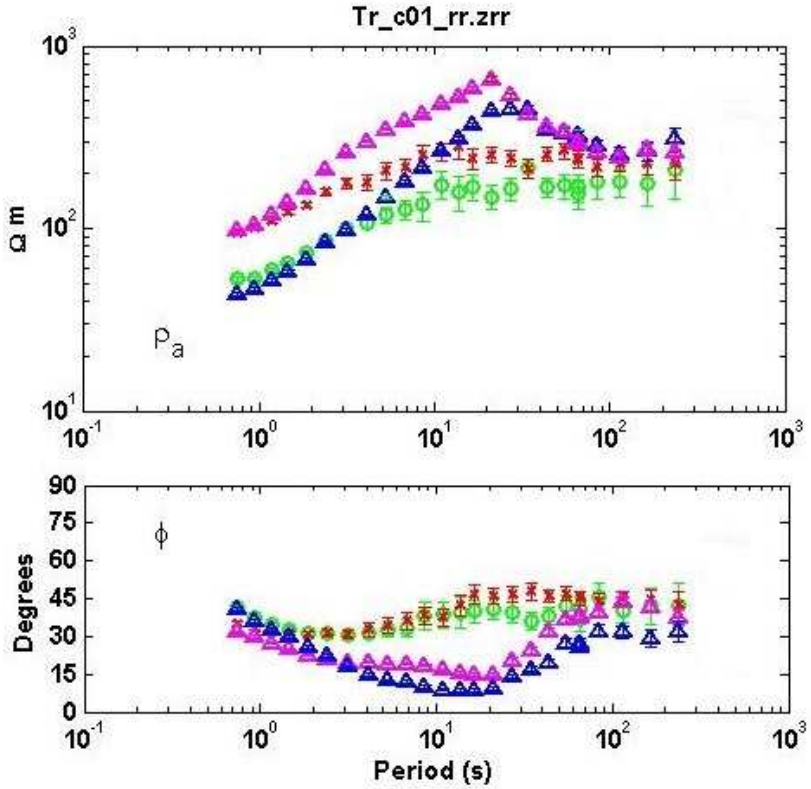

Figure 4.2: comparison between remote reference and single station curves for Tramutola. In blue and magenta are plotted respectively the xy and yx components of the single station curves. In green and red are plotted respectively the xy and yx components of the remote reference curves.

Figure 3.10 shows the results of the RR for Omalos using Tramutola as remote. In this case, it can be readily seen how the use of the remote reference does not allow any improvements but cause a worsening of estimates reliability in the period range 3s – 20 s where the MT curves becomes scattered and characterized by larger error bars. Remote Reference processing seems to suffer much more than the SS processing method when the local data contain obvious noise as in the case of Tramutola.

The comparison with the SS estimates is shown in fig 4.3.

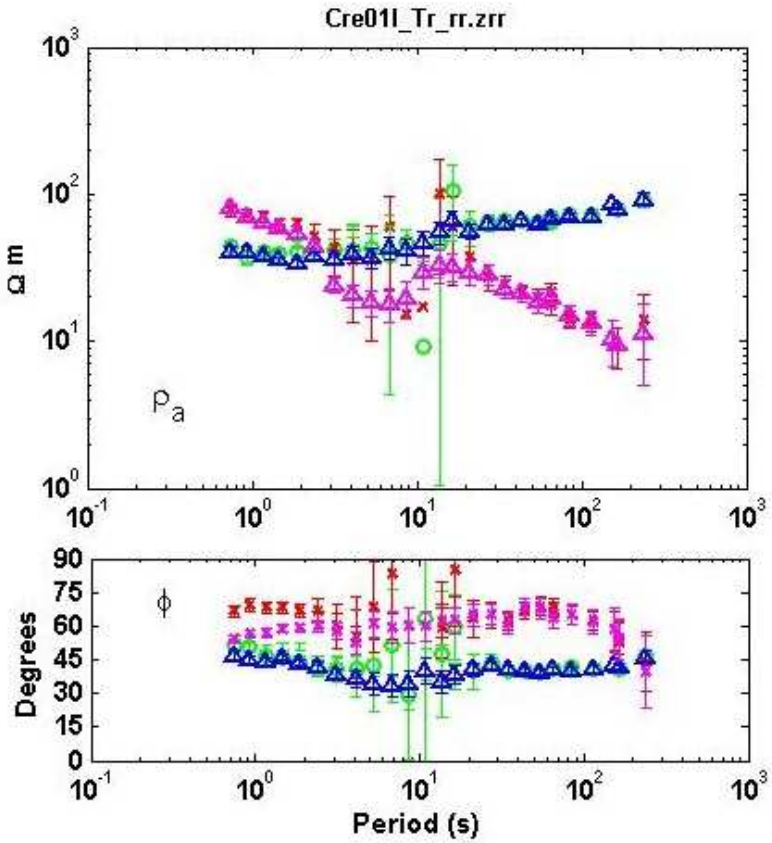

Figure 4.3: comparison between remote reference and single station curves for Omalos. In blue and magenta are plotted respectively the xy and yx components of the single station curves. In green and red are plotted respectively the xy and yx components of the remote reference curves.

Resistivity curves-Skin depth using the Bostick transfrom

Bostick transform on RR and SS curves are quite different. The use of the SS curves lead to an anomalous increase of resistivity which result in the presence of a high resistive stratum localized around 10 km depth. On the contrary the use of the RR curves results in smoother resistivity curves-Skin depth with no presence of any high resistive stratum.

The advantages of the presentation in the form shown in fig. 3.11 as compared to that shown in fig. 3.8, 3.9 are almost straightforward. Whereas the apparent resistivity and phase diagrams are hard to interpret in terms of subsurface structure, the Resistivity curves-Skin depth allows easy analysis of the results. In some aspects this presentation is equivalent to the resistivity-depth diagram and cross-section which is the end result of a routine inversion and interpretation procedure. It has, however, one important advantage over all conventional resistivity-depth diagrams. Unlike all others, it is not derived by the inversion of a single curve drawn to be the best approximation of resistivity and phase data. Rather, the depth section is derived point by point preserving the original character of the data. As shown in fig. 3.8, 3.9 it is easy to identify good or noisy portions of the data and identify missing sections in the data. In the conventional resistivity-depth section usually no indications of data quality and data characteristics are preserved. The obvious problem is that it is inherently only an approximation of the true resistivity-depth section. Although it may include indication of several parameters, it does not include other parameters of the data reduction process and, therefore, it should not be used by itself.

The strong difference between the output of Bostick transform applied to SS and RR MT curves shows the importance of obtaining the most reliable results from the MT process. In the case showed above, from the use of the SS curves can derive a total misleading result (i.e. the resistive deep stratum) that can distort the results of an MT survey.

"Electromagnetic seismograms"

Fluids residing in interconnected porosity networks have a significant weakening effect on the rheology of rocks and can strongly influence deformation along fault zones. The magnetotelluric (MT) technique is sensitive to interconnected fluid networks and can image these zones on

crustal and upper mantle scales. It has been considered that occurrence of earthquakes in the earth's crust is not only due to stress concentration but also due to decrease in effective confining pressure with pore pressure increasing in the source region. Such increase of pore pressure is expected to be induced by penetration of pressurized fluids in the crust. From a viewpoint of electrical resistivity (reciprocal of the electrical conductivity), both stress concentration and fluid penetration reduce the bulk resistivity in the upper or middle crust. If stress concentration raises pore pressure and pore connectivity, the bulk resistivity is expected to decrease (e.g.Bahr, 1997). On the other hand, fluid penetration also reduces the bulk resistivity, since the bulk resistivity of rocks depends largely on water content (e.g. Olhoeft, 1981). Hence it is natural to hypothesize that source region is electrically conductive and a good correlation exists between distribution of hypocentres and resistivity structure in the crust.

During the processing of the data from the MT-station in Omalos (Cre01.dat), a careful inspection of the electromagnetic time series has been done to look for bad data segment to exclude from the MT processing (see paragraph 3.6). Several anomalous waveforms similar to seismograms have been found mostly on the magnetic channels (fig. 4.4). The observed signals are not connected to the magnetotelluric source; they are not visible in fact on the Tramutola time series (fig. 4.5). The spike (highlighted by a red circle in fig 4.5) visible prior to the 2° event is most probably linked to local noise or to the sudden discharge of one of the capacitor of the magnetometer preamplifier.

A quick search on the Institute of Geodynamics (National Observatory of Athens) catalogue revealed the occurrence almost at the same time of two earthquakes (tab. 1) near Crete. The location of the epicentres of the two earthquakes is showed in fig. 4.6.

Earthquakes	Time (GMT)	Latitude (N)	Longitude (E)	Depth (km)	Magnitude (Local)
1^{st}	08:52:13.3	34.67°N	24.59°E	30	4.1
2^{nd}	08:54:06.5	34.74°N	24.59°E	32	3.9

Earthquake like these are not uncommon for the region of Crete placed in the proximity of the area in which the Africa plate subducts beneath the Aegean Sea plate (fig. 4.7), along the Hellenic arc, from the western Peloponnesus through Crete and Rhodes to western Turkey, at a rate of almost 40 mm/year. Shallow-focus earthquakes (focal depths less than 50 km) occur on

faults in the boundary-region of the two plates. From Crete to the west and northwest, most shallow earthquakes near the Hellenic-arc plate boundary are produced as the result of reverse or strike-slip motion, although some normal-faulting earthquakes do occur (Papazachos B. C., 1996)

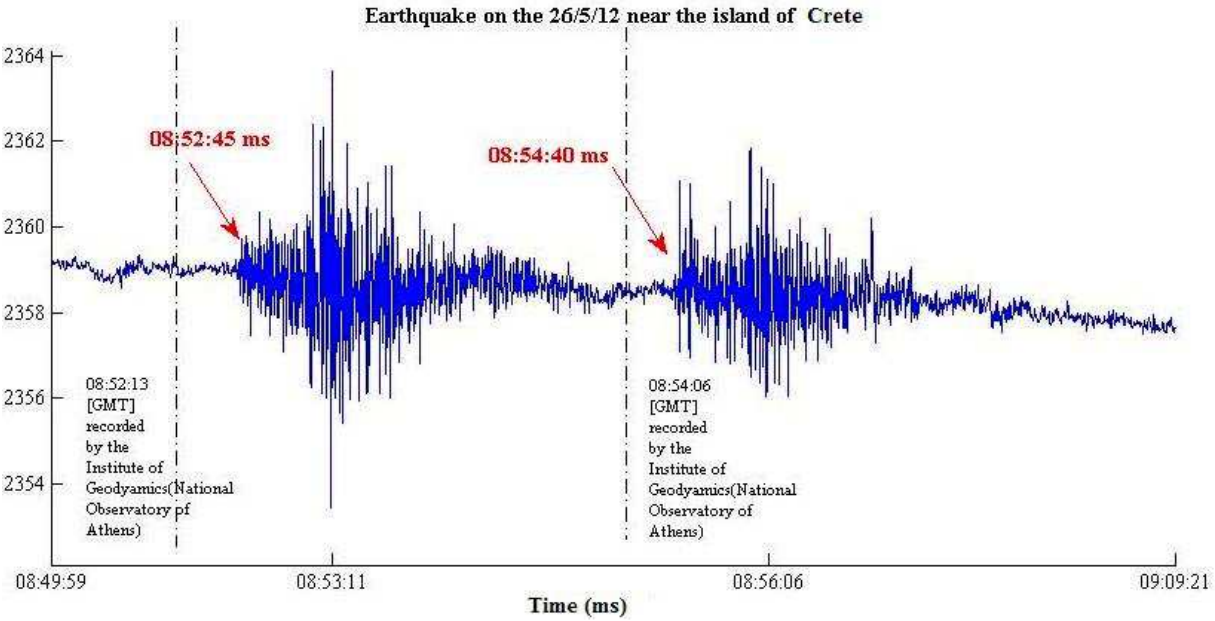

Figure 4.4: Seismogram like waveforms recorded from the magnetic channels of the MT monitoring station of Omalos. The figure also show with vertical dashed lines the occurrence time of the two earthquakes of tab.1

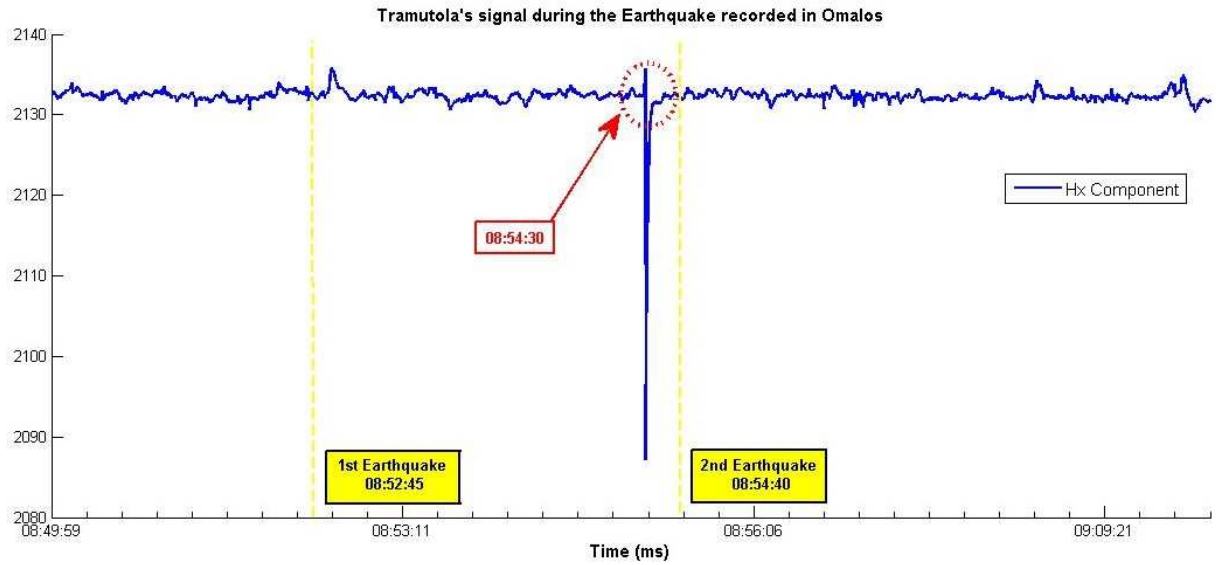

Figure 4.5: magnetic channels time series of the MT monitoring station of Tramutola. The figure also shows with vertical dashed lines the occurrence time of the two earthquakes of tab.1. The red dashed circle highlights an anomaly most probably linked to local noise or to the sudden discharge of one of the capacitor of the magnetometer preamplifier.

Figure 4.6: Maps showing the position of earthquake epicenters along with the location of the MT monitoring station of Omalos.

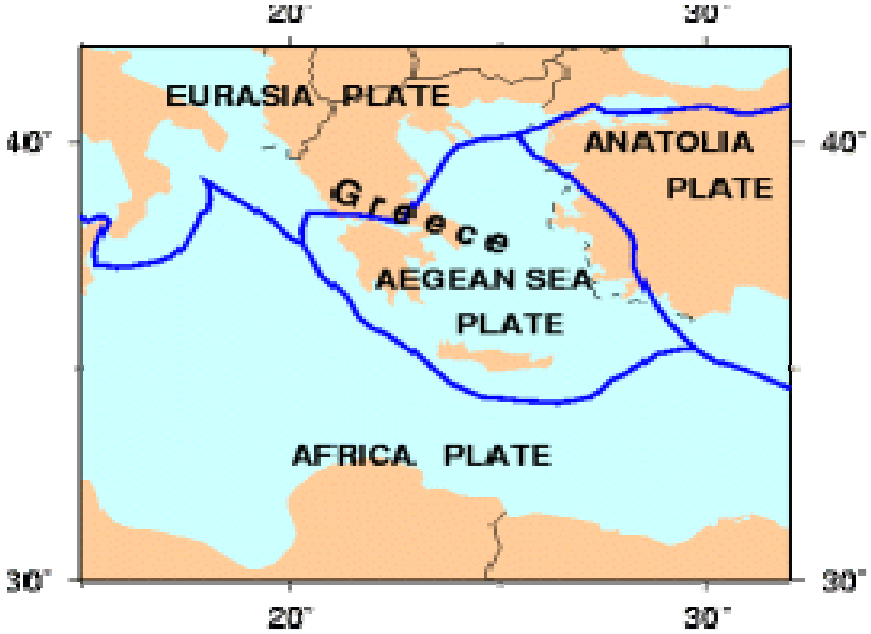

Figure 4.7: tectonic sketch of the eastern Mediterranean area (Greece, Tectonic Summary of Greece, Earthquake Hazards Program. Available on: http://earthquake.usgs.gov/earthquakes/world/greece/tectonic_summary.php)

The arrival time of the magnetic anomalous signals in the raw time series data, seems to be about 32 seconds after the origin time for the first earthquake and 34 seconds for the second one (as shown in fig.4.4). These delays could correspond to the arrival time of seismic waves to Omalos station. It is hence possible that these electromagnetic variations are associated with the passage of seismic waves and not to the earthquake generation and it could be linked to fluid movement induced by the seismic waves.

This phenomenon is not unknown in literature and the possible link with vibration of the MT sensors was excluded by Ujihara et al. (2004); Matsushima et al. (2002) observed electric and magnetic signals in association with Izmit earthquake, on 17 August 1999 M=7.4; Johnston et al. (2006) reported coseismic seismo-magnetic effects in association with the 28 September 2004 M=6.0 event; during the Bhuj earthquake occurred on 26 January 2001 (M=7.6), Abdul Azeez et al. (2009) observed significant changes in amplitude and frequency of magnetotelluric time series; Zlotnicki et al. (2006) documented anomalous electric and magnetic signals after, but even before, the seismic activity in the volcanic area; recently Romano et al. showed the occurrence of electromagnetic anomalies for really small magnitude earthquakes occurred in Pollino area (Italy).

CONCLUSIONS

The magnetotelluric method (MT) is a geophysical technique that utilizes the natural electromagnetic energy to electrically characterize Earth structures. For this reason and the huge frequency range from 〖10〗^(-5)- 〖10〗^4 Hz, with penetration depths extending from 10 m to 200 km in the last years, MT has been used to solve different geological problems, to monitor seismic areas and for a large number of applications. Due to the growing presence of cultural EM noise, robust techniques to data analysis are highly required to improve MT estimates reliability and, especially for monitoring purposes, their temporal stability.

In this thesis, it has been explored the possibility of applying the Remote Reference method along with its advantage between two MT monitoring stations: the Tramutola MT-station (Tr) installed in the Agri Valley by the IMAA-CNR institute and the permanent MT-station (Cre-01) in Omalos by the Laboratory of Geophysics and Seismology (TEI of Crete).

A visual inspection of the time series revealed very similar waveforms in the data recorded by the two stations (~ 1000 km far away from each other) confirming the possibility of using the RR method. So Cre-01 has been used as remote site for Tr and vice versa. The output of the RR has been hence compared with the Single Station processing technique results. By using Tr as remote station, the reliability of Cre-01 estimates is not improved. On the contrary, the quality of Tr MT estimates when calculated using Cre-01 as remote site is enhanced confirming the effectiveness of the RR method.

The possible consequences of using unreliable estimates in interpreting MT results have also been shown. Resistivity curves-Skin depth diagram calculated by applying the Bostick transform to the SS and RR Tr MT estimates resulted really different from the one based on the Single Station estimates (not reliable) indicating the presence of a strong resistive stratum around 10 km of depth.

As a curiosity more than a result, the last part of the thesis is focused on the electromagnetic anomalous signals recorded by the Cre-01 station after some earthquakes occurred in the Aegean Sea near Crete. The “electromagnetic seismograms” have been observed more than 30 seconds after the occurrence time of the earthquakes and are most probably linked to the passage of the seismic wave under the MT station.

Appendix A: The plane wave assumption

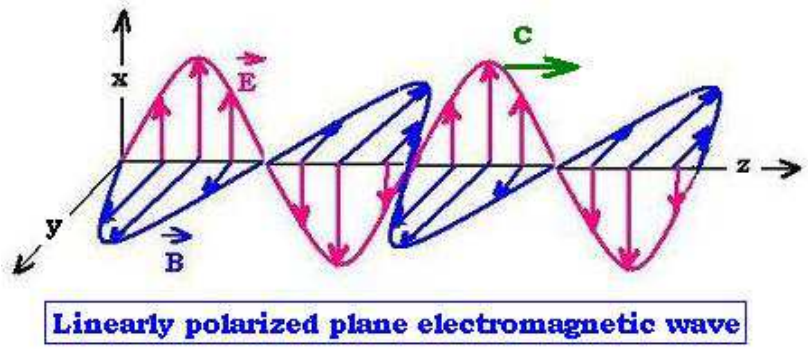

Figure A1: $\vec{B}$ is the magnetic field $\vec{c}$ is the electric field and z is the transmission direction.

In the physics of wave propagation, a plane wave is a constant-frequency wave whose wave fronts (surfaces of constant phase) are infinite parallel planes of constant amplitude normal to the phase vector (Fresnel A. J. 2001)

By extension, the term is also used to describe waves that are approximately plane waves in a localized region of space. For example, a localized source such as an antenna produces a field that is approximately a plane wave in its far-field region. Equivalently, for propagation in a homogeneous medium over length scales much longer than the wavelength, the "rays" in the limit where ray optics is valid correspond locally to approximate plane waves.

The wave equation for electromagnetic waves arises from Maxwell's equations. The form of a plane wave solution for the electric field is:

$$E = E_0 e^{i\omega t - \kappa z} \qquad \text{(A1.1)}$$

And that for the magnetic field:

$$B = B_0 e^{i\omega t - \kappa z} \qquad \text{(A2.2)}$$

Where k is the wavenumber (and wavelength, $\lambda = 2\pi/|k|$), ω is the angular frequency of the wave (period, $T = 2\pi/\omega$), and c is the speed of light. The magnetic field B is perpendicular to the electric field E in the orientation where the vector product E x B is in the direction of the propagation of the wave.

The plane wave assumption is fundamental to the MT technique, because it implies time invariance of the impedance tensor calculated from the recorded orthogonal electric and magnetic fields (assuming that the electrical conductivity structure of the Earth does not change and that signal-to-noise ratios are adequate).

Departures from the plane wave assumption occur in polar and equatorial regions owing to instabilities in the forms of the source fields that arise from complexities in the auroral and equatorial electrojet current systems. Depending on the degree of disturbance, departures from the uniform source can sometimes be circumvented by selection of a subset of undisturbed data. For example, night-time data is generally less disturbed than daytime data.

For periods of less than a day, the Earth's curvature has no significant effect on the plane wave assumption (Srivastava, 1965).Therefore, for the purposes of MT, it is sufficient to consider a flat-Earth model with electromagnetic fields described in Cartesian co-ordinates.

Appendix B: additional data

The main part of the thesis is focused on the analysis of Tramutola and Omalos MT monitoring stations. Along with this data, other two dataset have been analyzed. These two dataset, named Cre-02 and Cre-03, have been acquired with Cre-01 at the beginning of the monitoring activity in Crete (fig. B1). They were aimed to the characterization of two sites which were thought to be a possible alternative location to Omalos for the installation of the permanent MT monitoring station.

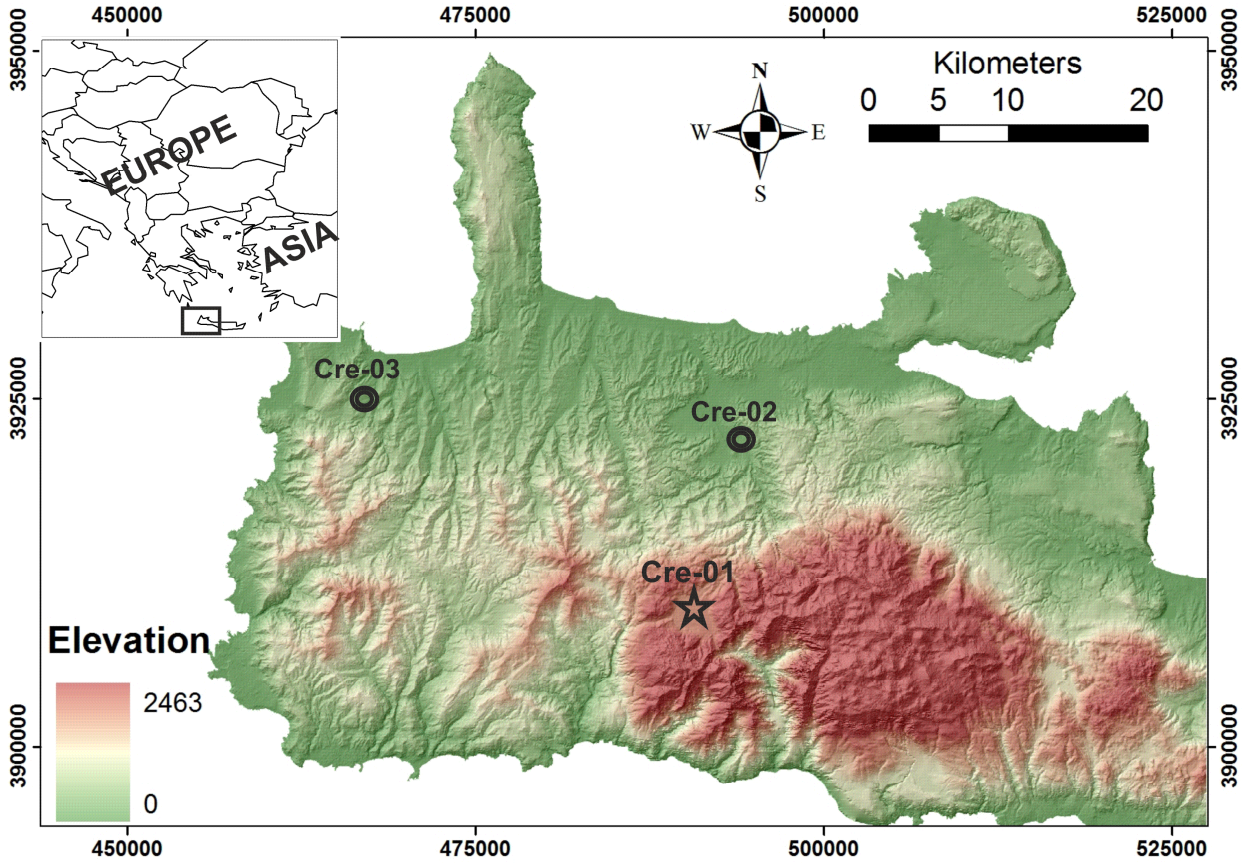

Figure B1: Map of the western part of Crete showing the position of the MT soundings. Star indicates the Magnetotelluric (MT) monitoring station in Omalos (Cre-01). Circles indicate the two MT surveys which took place in Fournes (Cre-02) and Kastelli (Cre-03).

Cre-02 dataset

The Cre-02 dataset was from the MT survey that took place in Fournes of Municipality Mousouron, located at a distance of 15.5 km Nothwest from the city of Chania and is built in the valley of Keriti exactly in the opposite direction from Lefka Ori which, lies in distance of 12 km southerly (Fournes in Chania, West Crete traditional villages. Available on: http://www.webcrete.net/index.php?option=com_content&task=view&id=481&Itemid=119)
The surficial geology is composed of Quaternary deposits that form depositional plains. Miocene to Pliocene sediments crop out in the central and the northwestern part of the study area and carbonates in the northeastern part. Dissected hills of phyllites and quartzites and a package of sedimentary rocks composed mostly of quartz-rich siliciclastic sediments with minor limestone and gypsum are observed mainly in the southwestern and southeastern part.
For Cre-02 dataset, (like in the case of Cre-01) the time series were registered through different bands, although only L and J bands (Low frequency and High frequency domain) were processed, with a total duration of three days.

Cre-02:
With acquisition starting time in 24/5/2012 at 11:00:00 to 27/5/2012 at 07:55:33 for the L-band.

Again, the J-band was recorded for each day separately during the morning and the night for 25 minutes each.
Like for Cre-01, before being processed with the Egbert's program, data have been reformatted, cleaned from the most evident noise effects and re-synchronized.
From a visual inspection of Cre-02 time series, we can detect a strong presence of noise affecting mainly the electric components which resulted in bad quality estimates for the single station processing and in the unsuitability of the data for the RR method. Single station results for the J and L bands are shown in figs B2 and B3.

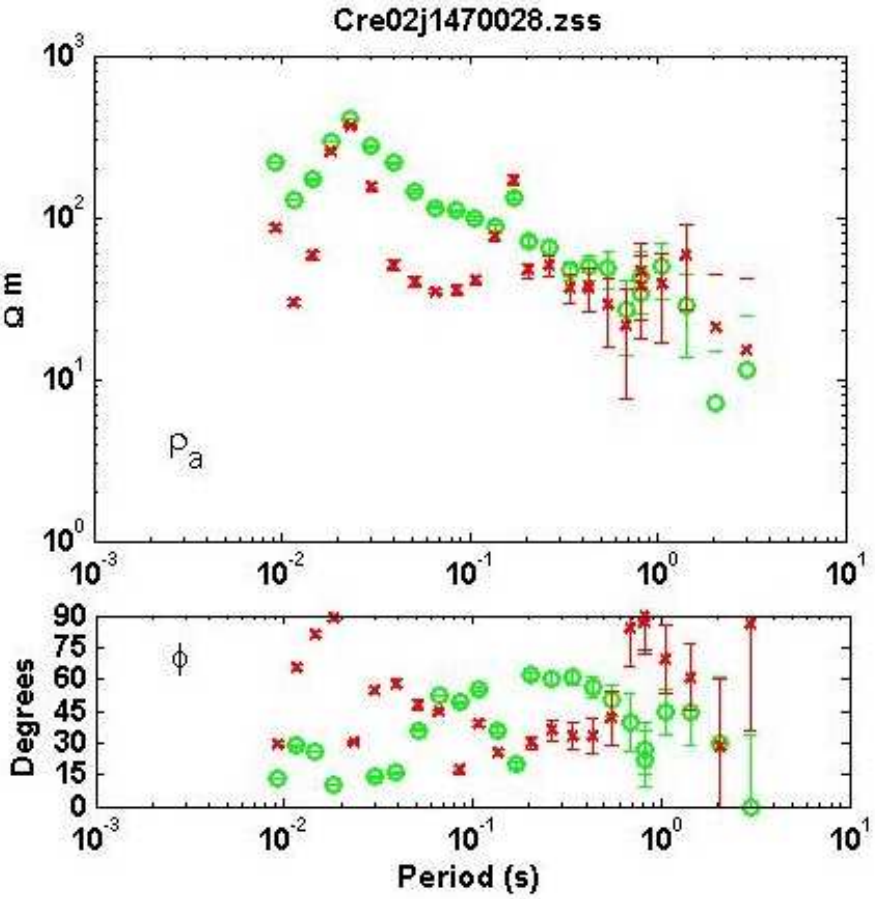

Figure B2: apparent resistivity and phase curves for the J band (sampling frequency = 500 Hz) obtained by means of single station MT processing. The green and the red curves are related respectively to the xy and to the yx components of the Impedance tensor.

Cre-02 curves are characterized by a scattered trend. As common the short period range estimates (J band) are more disturbed than long period estimates (L band). Estimates clearly suffer for the effects of EM cultural noise most probably connected to the presence of power line in the proximity of MT station. This can be testified by the scattered estimates of the yx curves (red curves) at sounding period around 0.019 s, and by the cusp, in the same period range, of the xy curves (green curves).

L band estimates (fig. B3) are less affected by cultural noise but clearly disturbed in the period range around 5s and 20s.

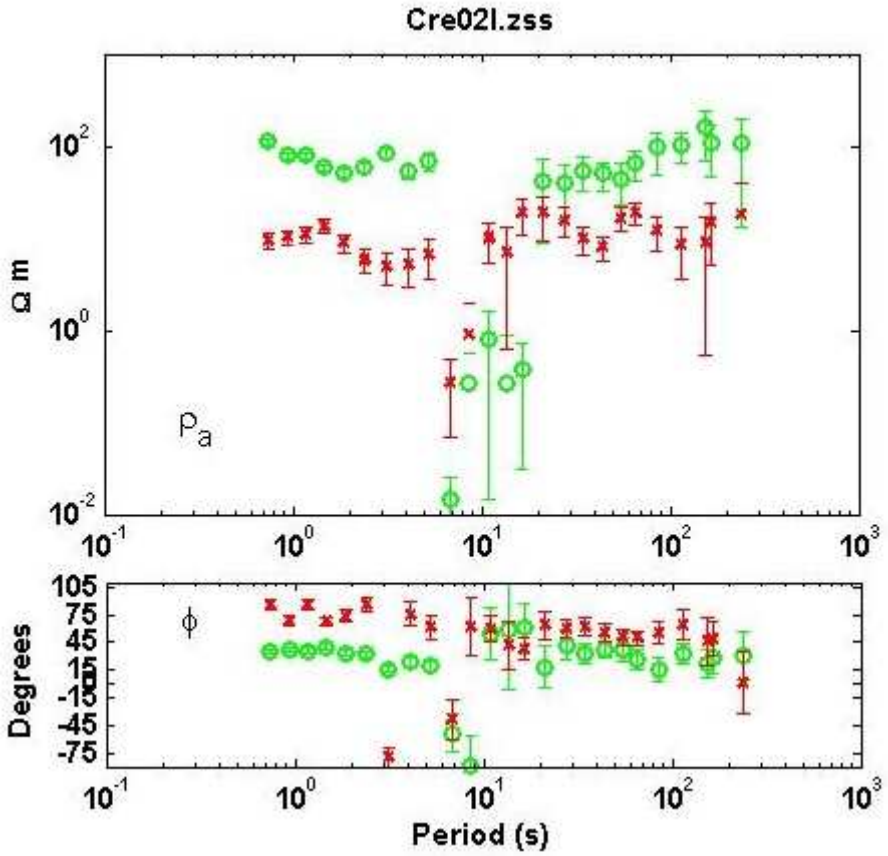

Figure B3: apparent resistivity and phase curves for the L band (sampling frequency = 6.25 Hz) obtained by means of single station MT processing. The green and the red curves are related respectively to the xy and to the yx components of the Impedance tensor.

Cre-03 dataset

The Cre-03 dataset was from the MT survey that took place in Kissamos or Kastelli Kissamou, which is a small town in West Crete, at the northwest end of the island. Kissamos, often still referred to by its earlier name of Kastelli, lies halfway along Kissamos Bay, 43 km from Chania. The nappe of the PhylliticQuartzitic series is possibly a preaalpine continental block, formed by phyllites, schists, quartzites, marbles, graywackes and gypsum. They are metamorphic rocks in high pressure/ low temperature conditions. The nappe lies tectonically on the formation of the platy limestones. In Chania Prefecture there are significant occurrences in the West of the Prefecture, in the Kissamos (Kasteli) area, in the southern part of the Prefecture

(PaleochoraChrissoskalitissa) department. In the lower members of this series (graywackes) gypsum is hosted.The thickness of the series exceeds 1,500 metres.

For Cre-03 dataset, the time series were registered through different bands, and only L and J bands (Low frequency and High frequency domain) were processed, with a total duration of three days.

Cre-03:

With acquisition starting time in 28/5/2012 at 13:00:00 to 31/5/2012 at 06:45:48 for the L-band.

Again, the J-band was recorded for each day separately during the morning and the night for 25 minutes each.

Before being processed with the Egbert's program, data have been reformatted, cleaned from the most evident noise effects and re-synchronized.

Like Cre-02, also Cre-03 time series are affected by a strong presence of noise affecting mainly the electric components. Single station estimates (fig. B4 and B5) are more reliable than RR estimates.

Power lines presence is readily visible in the J band where off-quadrant phases are also present (fig.B4). L band estimates (fig. B5) are less affected by cultural noise. A worsening of the estimates is visible between 3s and 20s.

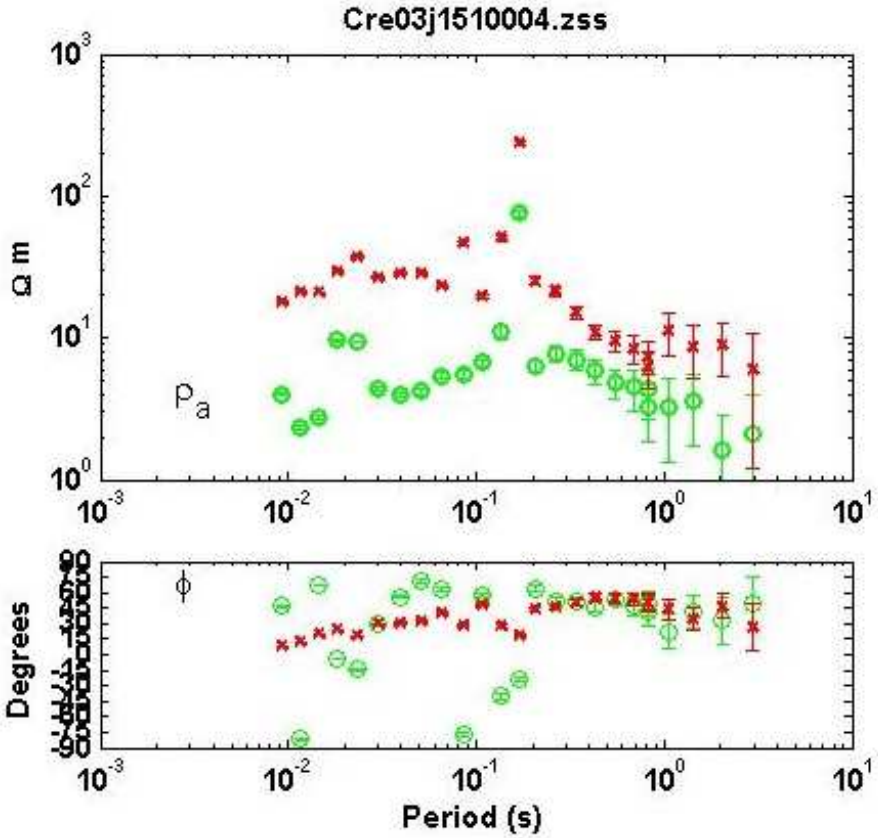

Figure B4: apparent resistivity and phase curves for the J band (sampling frequency = 500 Hz) obtained by means of single station MT processing. The green and the red curves are related respectively to the xy and to the yx components of the Impedance tensor.

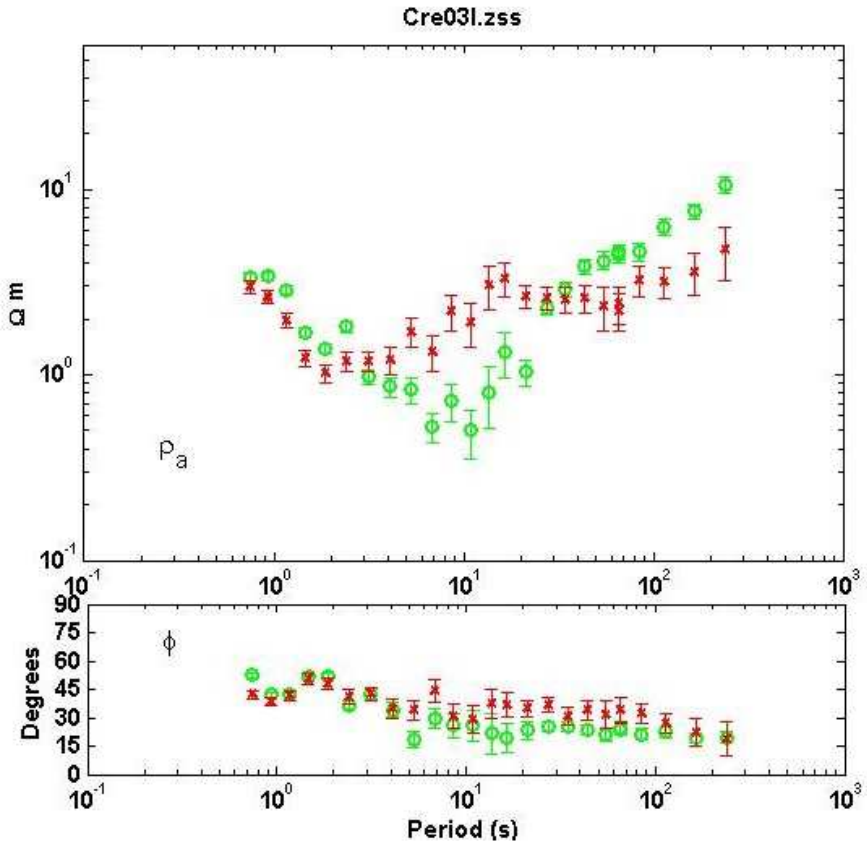

Figure B5: apparent resistivity and phase curves for the L band (sampling frequency = 6.25 Hz) obtained by means of single station MT processing. The green and the red curves are related respectively to the xy and to the yx components of the Impedance tensor.

REFERENCES

Abdul Azeez K. K., Manoj C., Veeraswamy K., and Harinarayana T. (2009) Co-seismic EM signals in magnetotelluric measurement — a case study during Bhuj earthquake (26th January 2001), India, Earth Planets Space, 61, 973–981.

Árnason K., 2007, The Magnetotelluric Method, Presented at Short Course II on Surface Exploration for Geothermal Resources, organized by UNU-GTP and KenGen at Lake Naivasha, Kenya.

Bahr K. and Simpson F., 2005, Practical Magnetotellurics, University Press, Cambridge

Balasco M., Lapenna V., Romano G., Siniscalchi A. and Telesca L., 2008, A new magnetotelluric monitoring network operating in Agri Valley (Southern Italy): study of stability of apparent resistivity estimates, Annals Of Geophysics 51.

Beltrando M, Peccerillo A, Mattei M, Conticelli S, and Doglioni C, 2010. Southern Apennines: structural setting and tectonic evolution, Journal of the Virtual Explorer 36, paper 13.

Cagniard, L., 1953, Basic theory of the magnetotelluric method of geophysical prospecting, Geophysics, v. 18, p. 605.

Chave, A.D., Thomson, D.J., 1989. Some comments on magnetotelluric response function estimation, J. Geophys. Res. 94, 14.215-14.225.

Cinque A., Patacca E., Scandone P. and Tozzi M. 1993 – Quaternary kinematic evolution of the Southern Appennines. Relationship between surface geological features and deep lithospheric structures. Ann. Geof., 36 (2), 249-260.

Egbert G.D. and Booker J.R., 1986, Robust estimation of geomagnetic transfer functions, Geophys J. R. astr. Soc., 87, 173-194.

Egbert G.D. and Livelybrooks D. W., 1996, Single station magnetotelluric impedance estimation: Coherence weighting and the regression M-estimate, Geophysics 61, 964-970

Egbert G.D., 1998, Matlab M-files for EMTF and multmtrn

Egbert, E. G., and Eisel, M., 1998, EMTF: Programs for Robust Single Station and Remote Reference Analysis of Magnetotelluric Data: UNIX (and PC) Version

Fasoulas Dr. G., 2004, The geology of the White Mountains, "Φουρόγατος" Magazine 54.

Fresnel A. J., 2001, Plane Waves and Wave Propagation.

Giano S. I., Lapenna V., Piscitelli S. and Schiattarella M., 2000, Elctrical oimaging and self-potential surveys to study the geological setting of the Quaternary slope deposits in the Agri high valley (Southern Italy), Annali di Geofisics 43, 409-419.

Goldberg S. and Rotstein Y., 1982, A Simple form of presentation of magnetotelluric data using the bostick transform, Geophysical Prospecting 30, 211-216.

Hamdan ., Economou N, Kritikakis G, Andronikidis N, Manoutsoglou E, Vafidis A, Pangratis P, and Apostolidou G, 2012, 2D and 3D imaging of the metamorphic carbonates at Omalos plateau/polje, Crete, Greece by employing independent and joint inversion on resistivity and seismic data, International Journal of Speleology 41 (2), 199-209.

Harinarayana T., 2008, Applications of Magnetotelluric Studies in India, Memoir Geological Society of India 68, 337-356.

Hersir G. P. and Árnason K., 2009, Resistivity Metods-MT, "Short Course on Surface Exploration for Geothermal Resources", organized by UNU-GTP and LaGeo, in Ahuachapan and Santa Tecla, El Salvador.

Hippolyte, J.-C., Angelier, J., Roure, F., 1994. A major geodynamic change revealed by Quaternary stress patterns in the Southern Apennines (Italy). Tectonophysics 230, 199–210.

Improta L., Ferranti L., De Martini P. M., Piscitelli S., Bruno P. P., Burrato P., Civico R., Giocoli A., Iorio M., D' Addezio G., and Maschio L., 2010, Detecting young, slow-slipping active faults by geologic and multidisciplinary high-resolution geophysical investigations: A case study from the Apennine seismic belt, Italy, J. Geophys. Res 11, B11307, 1-26.

Jones A. G., Chave A. D., Egbert G.D., Auld D. and Bahr K., 1989, A Comparison of Techniques for Magnetotelluric Response Function Estimation, J. Geophys. Res 94, 14.201-14.213.

Jones P.D., Briffa K.R., Barnett T.P. and Tett S.F.B. 1998, High-resolution palaeoclimatic records for the last millennium: interpretation, integration and comparison with General Circulation Model control-run temperatures, The Holocene 8,4 pp. 455–471

Kalisperi D.1, Makris J.P.1, Rigakis I.1, Romano G.2 and Vallianatos F.1,2013, Continuous Magnetotelluric Observations in Western Crete as a tool for the study of the Hellenic Subduction Zone, 13th International Congress of Geological Society of Greece.

Lydakis – Simantiris N. Pentari D., Perdikatsis V., Manutsoglu E., Moraetis D., and Apostolaki Ch., 2005, Mineralogical, geochemical and nutrient analysis of soils from Omalos polje -plateau, Western Crete, Proceedings of the International Workshop in Geoenvironment and Geotechnics 207-211.

Malinverno A. and Ryan W. B. F. 1986. Extension in the Tyrrhenian Sea and shortening in the Apennines as a result of arc migration driven by sinking of the lithosphere. Tectonics, 5,227-45.

Mallet R. 1862 the great Neapolitan earthquake of 1857. The first principles of observational seismology, Chapman and Hall (Publ.), London

Manutsoglu E., E. Spyridonos, A. Soujon and V. Jacobshagen (2001) 'Revision of the geological map and 3D modelling of the geological structure of the Samaria gorge region, W. Crete', Bulletin of the geological Society of Greece, vol. XXXIV/1, pp. 29-36.

Matsushima, M., Y. Honkura, N. Oshiman, S¸. Baris¸, M. K. Tunc¸er, S. B. Tank, C. C¸ erik, F. Takahashi, M. Nakanishi, R. Yoshimura, R. Pektas¸, T. Komut, E. Tolak, A. Ito, Y. Iio, and A. M. Is¸ikara (2002) Seimo-elecromagnetic effect associated with the Izmit earthquake and its aftershocks, Bull. Seismol. Soc. Am., 92, 350–360.

Montone, P., M. T. Mariucci, S. Pondrelli, and A. Amato (2004), An improved stress map for Italy and surrounding regions (Central Mediterranean), J. Geophys. Res., 109, B10410, doi:10.1029/2003JB002703.

Papazachos B. C., 1996, Large Seismic Faults in the Hellenic Arc, Annali Di Geofisica 5

Patacca E., Santori R., Scandone P. 1990. Tyrrhenian basin and Apenninic arcs: kinematic relations since late Tortorian times. Memorie della Societa Geologica Italiana 45: 425-451

Pomoni F. and Karakitsios V, 2002, Facies analysis of the Trypali carbonate unit (Upper Triassic) in central-western Crete (Greece): an evaporite formation transformed into solution-collapse breccias, Sedimentology 49, 1113–1132.

Pondrelli, S., S. Salimbeni, G. Ekström, A. Morelli, P. Gasperini and G. Vannucci (2006). The Italian CMT dataset from 1977 to the present, Phys. Earth Planet. Int., 159, 286-303; doi:10.1016/j.pepi.2006.07.008

Romano G., Balasco M., Lapenna V., Siniscalchi A. and Telesca L., 2012: Magnetotelluric monitoring of the Earth's crust in two seismogenic areas of Southern Italy (Val d'Agri and Pollino): preliminary results. 31th National Congress of the GNGTS –Gruppo Nazionale di Geofisica della Terra Solida

Srivastava S. P., 1965, Method of interpretation of magnetotelluric data when source field is considered. Journal of Geophysical Research Volume 70, Issue 4, pages 945–954, 15 February 1965

Smirnov M. Yu., 2003, Magnetotelluric data processing with a robust statistical procedure having a high breakdown point, Geophys. J. Int, 152, 1–7.

Ujihara, N., Honkura, Y., and Y. Ogawa (2004) Electric and magnetic field variations arising from the seismic dynamo effect for aftershocks of the M7.1 earthquake of 26 May 2003 of Miyagi Prefecture, NE Japan, Earth Planets Space, 56, 115–123.

Vafidis A, Manoutsoglou E, Hanmdan H, Andronikidis N, Koukadaki M, Kritikakis G, Oikonomou N, Spanoudakis N, 2004, Geophysical Prospecting on the plateau of Omalos Chania, Bulletin of the Geological Society of Greece, Proceedings of the 10th International Congress XXXVI

Zlotnicki, J., J. L. Le Mouel, R. Kanwar, P. Yvetot, G. Vargemezis, P. Menny, and F. Fauquet. (2006) Ground-based electromagnetic studies combined with remote sensing based on Demeter mission: A way to monitor active faults and volcanoes, Planet. Space Sci., 54, 541–557.

Explore West Crete : Kissamos. Available on: http://www.explorecrete.com/crete-west/EN-kissamos-kastelli.html

Fournes in Chania, West Crete traditional villages. Available on: http://www.webcrete.net/index.php?option=com_content&task=view&id=481&Itemid=119

Greece, Tectonic Summary of Greece, Earthquake Hazards Program. Available on: http://earthquake.usgs.gov/earthquakes/world/greece/tectonic_summary.php

Priore A., Geology and geomorphology of Upper Agri Valley. Available on: http://www.grumentum.net/en/geologia-e-geomorfologia-dellalta-val-dagri

Thiel S., 2008, Basics of the Magnetotelluric Method, Gh. 1-3. Available on: http://digital.library.adelaide.edu.au/dspace/bitstream/2440/48492/6/02chapters1-3.pdf